Masteroppgave

NTNU
Norges teknisk-naturvitenskapelige universitet
Fakultet for informasjonsteknologi og elektroteknikk
Institutt for elkrafteknikk

Steinar Halsne

Stability Assessment by Grid Impedance Method and Adaptive Control

Masteroppgave i Energi og Mlljø
Veileder: Assoc. Prof. Gilbert Bergna-Diaz
Juni 2019

NTNU
Kunnskap for en bedre verden

Steinar Halsne

Stability Assessment by Grid Impedance Method and Adaptive Control

Masteroppgave i Energi og MIljø
Veileder: Assoc. Prof. Gilbert Bergna-Diaz
Juni 2019

Norges teknisk-naturvitenskapelige universitet
Fakultet for informasjonsteknologi og elektroteknikk
Institutt for elkraftteknikk

NTNU
Kunnskap for en bedre verden

Abstract

In the last decades, the amount of power electronic converters in the electrical power grid has been growing rapidly. Increasing amounts of power is also being interfaced to the grid through such converters, as more and more renewable energy generation is included in the grid. The necessary increase in renewable power does, however, pose added challenges to the converters. This is because much of the renewable energy is being installed in a vast variation of grid conditions. There has been several accounts of unexpected instabilities in such systems. It is expected that resonance triggered between the converter and grid impedance is a likely cause of several of these events. Measures should be taken to avoid such unexpected instabilities if the desirable increase in renewable energy installation is to continue in a safe way.

One possible solution to assess this problem is the utilization of the so-called grid impedance method. In this thesis, the theoretical foundation of the grid impedance method is examined and explained. Based on this, a stability criteria is deduced. An important part of this stability criteria is knowledge of the equivalent impedance of the power system beyond the converter. For actual systems this impedance will be unknown and time-varying. Several possible methods for estimating this impedance are reviewed and the maximum length binary sequence method is selected, based on applicable criteria. The theoretical foundation of the grid impedance estimation method is examined and explained, before the method is implemented in both simulations and laboratory experiments. The grid impedance estimates exhibited a close match with theoretical values for simple simulations without constraints on sampling time or data-integrity. Furthermore, it was proven that the grid estimation method in its current form is not suitable for application in setups under the above data-integrity constraints. This does unfortunately also include the laboratory experiment. As a consequence of the former, it was decided that the stability assessment should be done exclusively by the use of theoretical values for the grid impedance to avoid false results. Under testing, the developed stability criteria, with theoretical grid impedance values, showed to be accurate within 16% of a real time simulation model. This was concluded to be acceptable as the simulation model contained elements present in actual systems, but which were not included in the analytical model. An original adaptive control procedure, based on the developed stability assessment, is also proposed in this thesis. The adaptive control is based on a graphical interpretation of the developed stability criteria. The proposed adaptive control performed well under testing as it improved the stability of the converter with minimal changes to its parameters.

Sammendrag

I løpet av de siste tiårene har mengden kraftomformere i det elektriske kraftnettet økt raskt. En økende del av effekten i nettet sendes også gjennom slike omformere da økende mengder fornybar kraft introduseres. Denne nødvendige økningen i fornybar kraft skaper derimot nye utfordringer for omformerne. Dette er fordi mye av den fornybare kraften installeres under veldig varierende nettforhold. Det har vært flere hendelser med uforutsett ustabilitet i slike systemer. Det anses som sannsynlig at flere av disse er forårsaket av resonans mellom omformeren og nettimpedansen. Tiltak burde iverksettes for å unngå slike hendelser om den ønskede økningen i fornybar kraft skal kunne fortsette på en trygg måte.

En mulig måte å oppdage slike problemer på er å bruke den såkalte nettimpedansmetoden. I denne avhandlingen undersøkes og forklares det teoretiske grunnlaget for denne metoden. Basert på dette blir også et stabilitetskriterie avledet. An viktig del av dette stabilitetskriteriet er å ha tilgang til den ekvivalente nettimpedansen utenfor omformeren. I virkelige systemer vil denne være ukjent og variere med tiden. Flere mulige måter å estimere nettimpedansen på undersøkes, og «maximum length binary sequence» metoden velges på bakgrunn av anvendbare kriterier. Det teoretiske grunnlaget for den valgte estimeringsmetoden undersøkes og forklares før den implementeres både i datasimuleringer og laboratorieeksperimenter. Den estimerte nettimpedansen viser tett korrelasjon med de teoretiske verdiene for enkle simuleringer uten begrensninger på samplingstid eller dataintegritet. Videre blir det vist at estimeringsmetoden på sin nåværende form ikke er egnet for bruk i oppsett med de nevnte begrensningene på dataintegritet. Dette er også gjelder også for de utførte laboratorieeksperimentene. På grunn av dette ble stabilitetsvurderingene gjort utelukkende ved bruk av teoretiske verdier for nettimpedansen for å unngå falske resultater. Stabilitetsvurderingen viste seg å være nøyaktig innenfor 16% av sanntidssimuleringer. Det konkluderes med at dette er et akseptabelt avvik da sanntidssimuleringene inneholder elementer som ikke inkluderes i de analytiske modellene. En original adaptiv kontroll prosedyre, basert på den utledede stabilitetsvurderingen, foreslås også mot slutten av avhandlingen. Tester viser at den adaptive kontrollen presterer bra da den øker stabiliteten til omformeren ved hjelp av minimale endringer av omformerens kontrollparametere.

Preface

This Masters Thesis was conducted at the Faculty of Information Technology and Electrical Engineering at the Norwegian University of Science and Technology in connection with the CINELDI project at SINTEF.

I would like to express my sincere gratitude and appreciation to my supervisor Assoc. Prof. Gilbert Bergna-Diaz and co-supervisors Dr. Raymundo Torres-Olguin, and Mr. Fredrik Göthner. Thank you for all your time and effort in helping me to create this thesis. Especially when faced with seemingly inexplicable problems your insights and experience has been invaluable. I would also like to thank all the guys and girls in the lab, for your willingness to help and share tips when the equipment did not function as expected. Also, a big thanks to Prof. Elisabetta Tedeschi and Prof. Dag Wessel-Berg for their understandable explanations of complicated theory. A big thanks must also be given to my good friend Mr Andreas Malmgård for agreeing to proofread this thesis.

Trondheim, 2019

Steinar Halsne

Contents

List of Figures

List of Tables

List of Abbreviations

2L-VSC	Two Level Voltage Source Converter
DG	Distributed Power Generation
FFT	Fast Fourier Transform
GHG	Green House Gasses
GIM	Grid Impedance Method
IGBT	Insulated Gate Bipolar Transistor
LTI	Linear Time-Invariant
MIMO	Multiple-Input-Multiple-Output
MLBS	Maximum Length Binary Sequence
PEC	Power Electronic Converter
PHIL	Power Hardware In The Loop
PI	Proportional-Integral
PLL	Phase-Locked Loop
PRBS	Pseudo Random Binary Sequence
PV	Photo-Voltaic
PWM	Pulse-Width-Modulation
RES	Renewable Energy Sources
SISO	Single-Input-Single-Output
SNR	Signal-to-Noise Ratio
WTG	Wind Turbine Generator

Chapter 1

Introduction

1.1 Background

Over the last few decades the power grid has been changing rapidly. Technological progress has vastly increased the population of Power Electronic Converters (PECs) in a variety of systems. They are commonly included in systems spanning from household appliances to power generation units. Furthermore, public awareness of the important topics of global climate change and the growing concentration of green house gasses (GHG) in the atmosphere has increased considerably. This has, in turn, spawned international agreements and multinational goals to reduce emissions and keep the global temperature increase below 2°C compared to pre-industrial levels [1, 2]. To achieve these goals, a substantial part of the reduction in GHG emissions are considered to have to come from the continued integration of Renewable Energy Sources (RES) [3]. As most RES are interfaced to the power grid through a PEC, the increasing penetration of RES will amplify the increase in PEC population. Moreover, as the share of renewables in the power mix increases and conventional power plants are replaced by RES, PECs will probably become dominant not only in the load side but also in power generation. This unprecedented condition may have a profound impact on the operation of the power system and must thus be explored.

Additionally, the power system does to an increasing extent incorporate, Distributed Power Generation (DG), such as rooftop Photo-voltaic (PV), small scale wind turbines, etc. That is, more of the power generation is shifted from the traditional large generation centers to smaller independent units with little or no centralized control. The shift towards renewable generation is thus making the power grid itself more diverse and dynamic. This will in turn also be true for the

conditions under which the PECs interfacing DG are supposed to operate. That is, the PECs must be able to operate in both a strong grid with several neighbouring converters as well as under weak grid conditions at the end of long radially connected power lines. The high level of controllability of the PECs undoubtedly adds a great deal of flexibility and possibilities to the power grid operation. However, there are also some adverse effects that must be considered. One of which is that several systems have experienced unexpected instabilities. Examples of this include Wind Turbine Generator (WTG) plants [4, 5, 6], Photo-Voltaic (PV) installations [7], residential distribution grids [8], etc. It has furthermore been suggested that a probable reason for several of these events is impedance interaction and resonance [9]. This is a challenge that should be overcome to facilitate the safe continued integration of RES into the power system and thus to continue the critical battle for reduced GHG emissions.

One proposed solution to this problem is to equip PEC to do stability assessments of its relation to the surrounding grid and to possibly adjust its behaviour accordingly. The reasoning behind this is mainly economical and related to versatility. As the conditions in the grid change or new equipment is installed, the stability assessment should ideally be repeated to ensure safe operation at the new operating point. It would be more convenient if the converter could do this by itself rather than having a centralized unit performing the analysis. Furthermore, if the PECs are able to operate more autonomously this would give a more resilient grid as there would be less dependency on centralized units. This is especially true in the scenario where the main grid fails but smaller units could be disconnected into islanded microgrids that operate alone. Moreover, this possibility of autonomous operation and independent stability assessment would facilitate so called plug-and-play capabilities. That is, with plug-and-play capabilities the PEC could be installed under any normal grid conditions and operate as intended with no need for site-specific information beforehand. This would help reduce cost and increase the competitiveness of RES. In this regard it would also be preferable if the stability assessment method could be implemented without any considerable need for additional hardware or upgrades to a generic PEC. These mentioned notions will serve as a backdrop and guideline for the choice of methods made in this thesis.

One candidate for such a stability assessment method is the Grid Impedance Method (GIM) as it will be denoted in this thesis. The exploration and examination of stability assessment by this method will be the main focus. Additionally, it should be noted that even though the work and discussions in this thesis could be valid for PECs in a variety of applications, it is chosen to focus the considerations towards the implementation in relation to RES and microgrids.

The next section will briefly clarify the considerations and assumptions that would make traditional stability assessment methods insufficient for the applications assumed herein. Thus, it will help corroborate the examined method's possible value beyond academical interest.

1.2 Stability Assessment Methods

Several well known and accepted methods for stability assessment already exist, and it will perhaps not be obvious why alternatives, such as GIM, may be needed. This section will briefly highlight the main deficiencies of the traditional methods and corroborate one last guideline that will be used throughout this thesis.

Traditionally, small signal stability analysis in the power grid has most often been done either by using the state-space modeling or by transfer function analysis [10]. In state-space modeling, an extensive set of equations describing the power system and its components is created and analyzed. This will yield a very detailed representation of the system and its stability, but it will at the same time be quite computationally demanding. This is especially true when the system size grows. The traditional transfer function approach is simpler as it neglects many of the internal states and yield input/output characteristics. However, the main drawback of the two former methods is that they both require extensive knowledge of the power grid components and, more importantly, the controls of the units therein [10]. This information is not readily available, especially since controller details are often considered confidential information by suppliers. Because of this, alternatives that do not rely on such information should be explored to yield results of sufficient accuracy. One such method is the grid impedance method.

Additionally, as will become apparent later in this thesis, the value of the grid impedance plays a profound role in the stability of the system with regard to resonance. As it turns out, the grid impedance exhibits considerable variation, not only in months or weeks, but also within a single day and a single hour. One example of this is shown in figure 1.1.

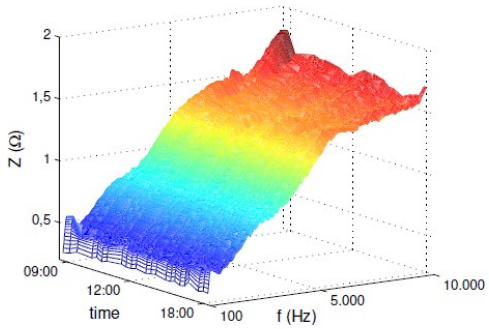

Figure 1.1: Impedance variation over the course of one day [11]

Because of this it can be considered that one time or irregular stability assessments will not be sufficient to guarantee stability. This is also supported by the unstable cases mentioned previously. Therefore, the stability assessments should be carried out online. Furthermore, if the PEC is part of a possible microgrid and an islanding event occurs, the equivalent grid impedance could change drastically within a few moments. Because of this, the stability assessment method should preferably yield its result as quickly as possible to allow the PEC to adjust before unstable conditions are reached. Quick evaluation times will thus be a final guideline for the following work herein. Furthermore, it should be noted that to achieve this

in line with the other guidelines of not needing considerable additional upgrades to a generic PEC, the implemented algorithm should be kept from becoming too computationally heavy. This would also further disqualify the traditional methods above.

1.3 Objectives, Scope of Work, and Methodology

1.3.1 Objectives

The objectives of this thesis are to:

1. Examine the theoretical background of the grid impedance method
2. Deduce a stability criterion associated with this method
3. Find a suitable method for grid impedance estimation, that can be used in online impedance-based stability assessment.
4. Examine the grid impedance estimation method's suitability for real time implementation
5. Propose a simple adaptive control to act on the information from the stability assessment
6. Conduct simulations and laboratory experiments that can make some indications on how well the proposed methods work

1.3.2 Limitations on Scope of Work

To be able to achieve the main goals of this thesis within the permitted time the following restraints on the scope of work are made:

The three phase electrical system under study will at all times be assumed to be balanced. Any imbalances occurring for any reason are considered to be outside the scope of this thesis.

The DC side voltage of the converter will at all times be assumed constant.

Also related to the former restraint, the inclusion of any control loops in the converter, outside the current controller and proposed adaptive control, are neglected.

The converter is considered to be connected to a grid with a constant voltage source at all times.

A converter could operate in current controlled mode or voltage controlled mode. That is, either the current or the voltage on the output of the converter is measured and controlled. In the following, the converters are exclusively considered to

operate in current controlled mode. This is because it is the most common mode of operation for such systems when connected to the grid [12].

Optimization of the stability assessment method with regard to time use, will be considered beyond the scope of this thesis. However, the modeling choices are made so that this will be a possibility in a further work, in accordance with the guidelines presented in the introduction. The former statement will apply to both the numerical evaluation of the converter model and to the implementation of the grid impedance estimation method.

Optimization of the accuracy of the grid impedance estimation, beyond what is proposed in the reviewed literature, is considered to be outside the scope of this work in accordance with the previously stated objectives.

1.3.3 Methodology

The methodology adopted for this thesis in order to achieve the goals will be as follows:

First, a thorough theoretical foundation of the examined topic will be established through literature review and own deductions. Then, appropriate analytical expressions are created before the deduced relations are implemented and tested through computer software tools, simulations or laboratory experiments. The results of the tests are then evaluated. If the results are found to be unacceptable another iteration of the above steps will be conducted if time permits. If time does not permit new iterations, suggestions will be made on how this could be done in a further work. Note that all steps and iterations will not be explicitly shown in this thesis. The main results of the work will rather be presented towards the end of the document.

In the following work it was chosen to prioritize the development of the stability criteria first, the implementation of the grid impedance estimation method second, and the work with the adaptive controller third. The transition between the three is guided by the limitations on the scope of work presented above, although not explicitly stated in the text.

Chapter 2

Grid Impedance Method

The grid impedance method is the main topic of this thesis and its key features will be elaborated in this chapter. First the outline of the method is explained in a simplified manner. Then the needed analytical models are established and combined into the complete model considered herein. Lastly the stability criterion is derived based on the developed equivalent model.

2.1 Basic Introduction to the Grid Impedance Method

This section will briefly and in a simplified manner introduce the main concepts of the grid impedance method. This is done to provide an overview for the more detailed elaborations in subsequent sections. The discussion in this section is to a large extent based on [13, 14].

To guide the discussion, consider the system shown if figure 2.1 where PEC is interfacing a DC-source to the AC-grid, through an LCL-filter.

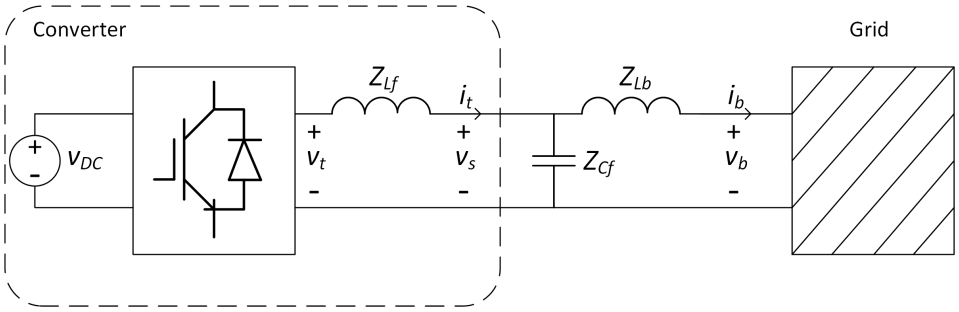

Figure 2.1: One line diagram of a generic converter connected to the grid through an LCL-filter

The DC-side could be a power source such as a PV installation or some other system, this is simply represented as a constant DC source in the figure. The converter is also chosen to be connected to the grid via an LCL-filter. However, for practical reasons, only the first inductor is included within the system boundaries of the converter while the rest of the filter is included in the grid.

The system beyond the converter switches can be converted to the form shown in equation 2.1

$$i_t = Y_f \cdot v_t - Y_f \cdot v_s \tag{2.1}$$

where v_t is the voltage at the output of the converter switches, i_t is the converter output current, v_s is the converter terminal voltage, while Y_f is the equivalent admittance of the filter inductor.

This equation can be visualized as a block diagram as shown in figure 2.2.

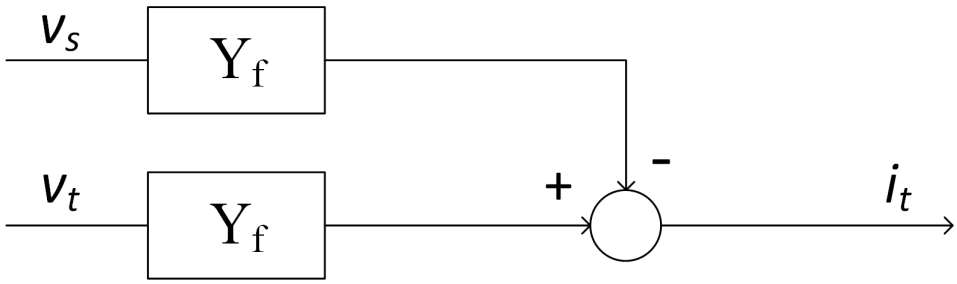

Figure 2.2: Equation 2.1 visualized as a block diagram

As mentioned previously, the converter could operate in current controlled mode or voltage controlled mode. That is, either the current or the voltage on the output of the converter is measured and controlled. Only the current controlled mode is used here in accordance with the scope of work. However, it should be noted that the later derived stability criterion would be drastically different and opposite if the converter was operating in voltage controlled mode [12]. The latter is included only for reference and will not be included in this thesis.

Assuming the current controlled mode, a current feedback loop and some controller is added to yield the current controlled converter model depicted in figure 2.3. Here G_{cli} denotes the closed loop transfer function from current error signal to output voltage, including current controller action.

It would also be possible to add additional outer control loops such as DC-voltage control and power controllers. However, the principle would be the same. Thus for simplicity, only the inner current control is considered in the following models. In this regard it should also be noted that the DC-link voltage will thus be assumed to be held constant by some other, outer control loop which is not included.

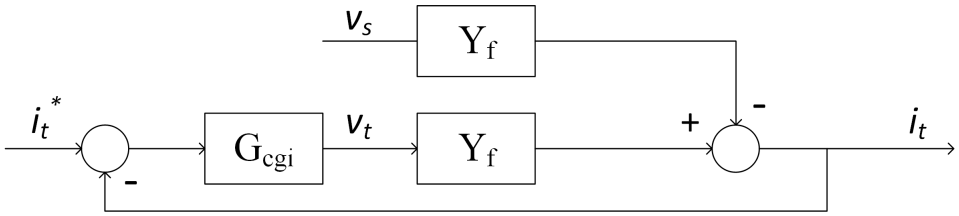

Figure 2.3: Simple current controlled converter model

By rewriting the above block diagram, the converter model can be transformed into a Norton equivalent. If this is connected to a Thevenin equivalent of the grid, the system shown in figure 2.4 can be created. Here Y_{oi} denotes the equivalent admittance of the converter, while Z_g denotes the equivalent Thevenin impedance of the grid.

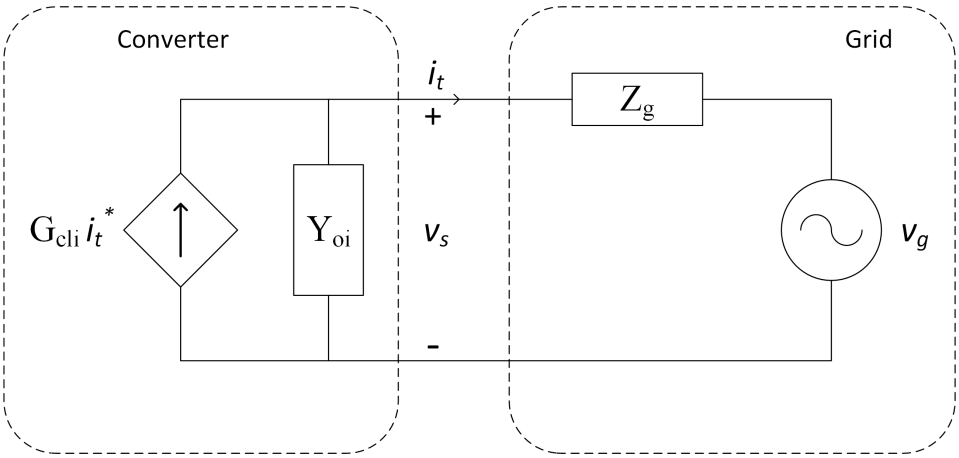

Figure 2.4: Norton equivalent of converter connected to a Thevenin equivalent of the grid

The last step in this deduction is to apply circuit analysis to this linear circuit model. This would yield equations which could be combined into the block diagram shown below in figure 2.5. It can be observed that if the two terms on the left are stable, then the stability of the entire system is governed by the so-called minor loop gain $Y_o \cdot Z_g$. That is, the stability of the system will be governed by the interaction between the equivalent converter admittance and the equivalent grid impedance. The two terms on the left being stable would translate into the current source being stable when unloaded, and the converter equivalent admittance is stable when supplied from an ideal grid [12]. This would in most cases be true as it in practice would be a prerequisite for being allowed to connect to the grid.

Furthermore, provided that the system may be approximately modeled as a linear time-invariant (LTI) system, the stability can be assessed by use of the well known Nyquist stability criterion[15]. Additionally, assuming the grid to be stable, then both Y_o and Z_g are assumed stable. Thus their product will have no unstable poles, i.e. no poles in the right-hand part of the complex number plane [15]. Therefore, the stability criterion is simplified to require that the Nyquist plot of $Y_o \cdot Z_g$ does not encircle the point (-1,0) in the complex number plane.

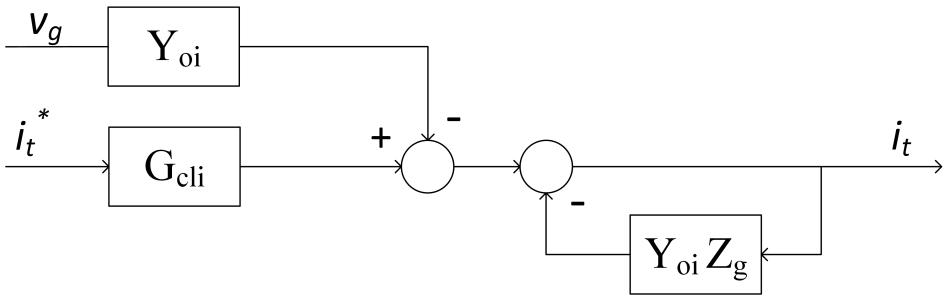

Figure 2.5: Block diagram equivalent of figure 2.4

From the discussion presented in this section, it is obvious that the grid impedance method has some attractive features that distinguishes it from the more traditional methods mentioned in the introduction. One of which is the relative ease of evaluation of the stability criteria. The grid impedance method only requires evaluation of the Nyquist contour of the minor loop gain, which furthermore may be implemented as a graphical criterion. This is in strong contrast to the possibly vast sets of equations that must be solved for the state space method. The computational burden would probably be drastically reduced in any but a few very simple cases. Additionally, the grid impedance method does not require extensive information about the surrounding grid as opposed to the mentioned traditional methods. It only needs to establish the two equivalents Y_o and Z_g. The details of this will become clear throughout this thesis.

Lastly, it should be noted that to make the model approximately LTI, as required to utilize the Nyquist criterion, small signal modeling is adopted as the main approach in this thesis. Small signal analysis refers to analyzing a system for small perturbations about some steady-state operating point within which the system can be approximated as being linear [10]. Therefore, the stability assessment presented herein will obviously only be valid for small signal considerations.

This section briefly introduced the main idea behind the grid impedance method and outlines several of the steps to be made in this thesis to establish the full stability assessment tool. The next sections will establish the converter model to be used and expand on some practical considerations. Then the different model pieces will be combined and a converter equivalent corresponding to that in figure 2.4 is established and a stability criteria is deduced. The subsequent chapter will

then be concerned with determining the grid equivalent Z_g.

2.2 Average Model of The Two Level Voltage Source Converter

This section will present the derivation of one of the main building blocks in the stability assessment method of this thesis, namely the average model of a two level voltage source converter. In the subsequent section this model is expanded by the inclusion of controllers, grid synchronization and delays to yield the final converter model

The basis for the converter modeling in this thesis will be a conventional two level voltage source converter (2L-VSC) as they are commonly used in various systems. This section will provide the basis for the converter modeling, derive the relevant equations, and clarify the modeling choices made in a brief and simplified way. This is done for completeness and to highlight the key features that must be taken into account in later derivations and considerations. The modeling of the 2L-VSC herein is based on known circuit theory, and more specifically what is reported in [16].

The starting point is the full-bridge converter with two voltage levels and output filter connected to the grid shown in figure 2.6. Note that, as mentioned in section 2.1 only the first inductor is considered as part of the converter while any extra filter capacitor-inductor branch is considered as part of the grid.

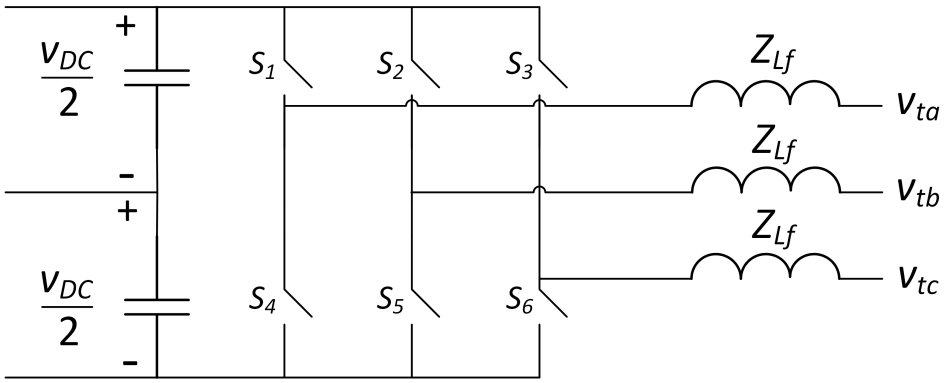

Figure 2.6: Simplified diagram of a two-level voltage source converter

Consider the first leg, connected to phase a. There are two possibilities under ideal operation: S_1 is on ($S_1 = 1$) while S_4 is off ($S_4 = 0$). Then the voltage at the terminal of this leg, V_l, equals $V_p = \frac{V_{DC}}{2}$. The other possibility is when S_1

is off ($S_1 = 0$) while S_4 is on ($S_4 = 1$). Then the leg terminal voltage, V_l equals $V_n = -\frac{V_{DC}}{2}$.

From the above discussion it is clear that the switch positions and grid side voltage of the converter leg a can be described as shown in equation 2.2 and 2.3 respectively.

$$S_1(t) + S_4(t) \equiv 1 \tag{2.2}$$

$$v_l(t) = \frac{V_{DC}(t)}{2} \cdot S_1(t) - \frac{V_{DC}(t)}{2} \cdot S_4(t) \tag{2.3}$$

At this point it should be noted that to establish equations 2.2 and 2.3, any turn-on and turn-off transients and corresponding dead-time are neglected. The dead-time term refers to the time period where both the upper and lower switch of a leg are kept off while the switch is going into blocking mode. This is to ensure that both switches will not conduct at the same time and cause a flash-through.

A per phase circuit equation of the converter in figure 2.3 can generally be written as

$$L \cdot \frac{d}{dt} i(t) + R \cdot i(t) = v_l(t) - v_t(t) \tag{2.4}$$

where i is the current flowing out of the converter, v_l is the phase to neutral voltage at the leg terminal, and v_t is the phase to neutral voltage at the converter terminal. That is, between the first inductor and the CL-branch of the filter. Furthermore, L is the filter inductor inductance and R is a lumped parameter of the resistance along the path. These two parameters are combined into the filter impedance Z_{Lf} in figure 2.6.

Equation 2.3, and thus equation 2.4, is discrete. This is inconvenient in the further modeling as conventional control theory is based on continuous equations. Therefore, the switching action is approximated by an average model in order to make the converter model of equation 2.4 continuous. In the subsequent discussion it is assumed that the switches are controlled by a pulse-width-modulation (PWM) scheme. The average model is introduced by considering the switch command signal S from the PWM to be constant over one switching period and approximated by its average value over this period. This average value is referred to as the duty ratio, d, and is defined as the fraction of the full switching period when the switch command signal yields on. This approximation is considered acceptable in conventional power electronics theory as long as the frequency of the carrier signal of the PWM is much higher than that of the modulating [17]. Utilizing the above assumption and the assumption of the switches of one leg to have opposite switching status in equation 2.2, the average switching status can be written as shown in equations 2.5 and 2.6,

$$\bar{S_1}(t) = d \tag{2.5}$$

$$\bar{S_4}(t) = 1 - d \tag{2.6}$$

where the overbar indicates averaged value.

Equation 2.3 can thus be approximated as shown in equation 2.7.

$$\bar{v_l}(t) = \frac{V_{DC}(t)}{2} \cdot (2d - 1) \tag{2.7}$$

Finally, utilizing the above, equation 2.4 can be rewritten into the well known averaged model version in equation 2.8

$$L \cdot \frac{d}{dt} i(t) + R \cdot i(t) = \frac{V_{DC}(t)}{2} \cdot m(t) - v_t(t) \tag{2.8}$$

where the bars have been dropped for compactness and $(2d - 1)$ is denoted by m for convenience.

At this point, the ramifications of the modeling should again be noted. The simplified derivation so far has resulted in a simple per phase model that is continuous in time. This will undoubtedly simplify subsequent modeling and analysis. However, to achieve this not only is the turn-on/turn-off dynamics neglected, but also any switching dynamics altogether. This does of course lower the fidelity of the developed model to actual physical systems, especially for high frequencies. Nonetheless, based on the gain in computational time, simplicity and the results presented later in this thesis, the loss of information is considered acceptable.

Additionally it should be noted that equation 2.8 will only represent a singe phase, while the addition of two additional equations each shifted 120° in time will constitute the entire three phase model. This model will contain sinusoidal signals related to the natural abc-reference frame. Because of the incessant variation of the signals, a control scheme based on the use of linear control theory and proportional-integral (PI) controllers will not be able to follow a sinusoidal reference signal without considerable deviations [15, 16]. There are several possible solutions to this problem, each with its own advantages and disadvantages. The approach adopted herein is to transform the model equations from the natural reference frame to the synchronously rotating dq reference frame. This allows the use of linear control theory as all sinusoidal voltage and current signals are transformed into DC-signals. Some key features and further details on this are presented in Appendix A. A thorough explanation on how the transformation is derived and performed can be found in [16].

To perform the transformation from abc to dq domain the well known Parks transformation, shown in equation 2.9, is used [16].

$$\begin{bmatrix} v_d \\ v_q \end{bmatrix} = \frac{2}{3} \cdot \begin{bmatrix} \sin(\theta) & \sin(\theta - \frac{2\pi}{3}) & \sin(\theta + \frac{2\pi}{3}) \\ \cos(\theta) & \cos(\theta - \frac{2\pi}{3}) & \cos(\theta + \frac{2\pi}{3}) \end{bmatrix} \cdot \begin{bmatrix} v_a \\ v_b \\ v_c \end{bmatrix} \tag{2.9}$$

Here θ denotes the angle between the d-axis and the system voltage phasor. Furthermore, θ is chosen to be zero degrees in this thesis. See Appendix A for further elaborations on this.

The results of the transformation is shown in equation 2.10 and 2.11 where all variables now are DC quantities.

$$\frac{d}{dt} i_{td} = \omega_0 \cdot i_{tq} - \frac{R}{L} \cdot i_{td} + \frac{V_{DC}}{2L} \cdot m_d - \frac{v_{sd}}{L} \tag{2.10}$$

$$\frac{d}{dt} i_{tq} = -\omega_0 \cdot i_{td} - \frac{R}{L} \cdot i_{tq} + \frac{V_{DC}}{2L} \cdot m_q - \frac{v_{sq}}{L} \tag{2.11}$$

Equation 2.10 and 2.11 also highlight one of the disadvantages of utilizing the dq-reference frame, namely the coupling terms between the d- and q-axis currents. That is, any change in the d-axis current will have an effect in the q-axis current and vice versa. This must be accounted for in the design of the control system presented in section 2.3.

A final step in this derivation will be to convert equation 2.10 and 2.11 to small signal equations. As the dc-voltage is assumed to be constant in this thesis, there is no need for linearization as the equations already are linear. Therefore, the change to small signal equations will not result in any change in the equation structure, only in a change of variables. However, a very brief discussion is included here for completeness. Also note that as the derivation would be the same in the d- and q-axis, only the d-axis derivation is included.

The small signal approach considers systems that in steady-state are assumed to behave linearly subjected to some small disturbance. In the following, capital letters used for variables will denote steady-state values while tilde notation is used to denote a small perturbation about the operating point. Utilizing this notation, all the signals in equation 2.10 would generally be comprised of its steady-state value and possibly some small disturbance as shown in equation 2.12

$$\frac{d}{dt}(I_{td} + \tilde{i}_{td}) = \omega_0 \cdot (I_{tq} + \tilde{i}_{tq}) - \frac{R}{L} \cdot (I_{td} + \tilde{i}_{td}) + \frac{V_{DC}}{2L} \cdot (M_d + \tilde{m}_d) - \frac{(v_{sd} + \tilde{v}_{sd})}{L} \tag{2.12}$$

Consider the case where there are no perturbations. Equation 2.12 will then only contain the steady-state values. As the time derivative of the constant on the left hand side is zero, so is the sum of steady-state terms on the right hand side. Thus,

only the perturbation terms of equation 2.12 survives in the general case and the small signal model can be reduced to the form shown in equation 2.13.

$$\frac{d}{dt}\tilde{i}_{td} = \omega_0 \cdot \tilde{i}_{tq} - \frac{R}{L} \cdot \tilde{i}_{td} + \frac{V_{DC}}{2L} \cdot \tilde{m}_d - \frac{\tilde{v}_{sd}}{L} \tag{2.13}$$

Similarly, for the q-axis equation 2.11 can be written as in equation 2.14

$$\frac{d}{dt}\tilde{i}_{tq} = \omega_0 \cdot \tilde{i}_{td} - \frac{R}{L} \cdot \tilde{i}_{tq} + \frac{V_{DC}}{2L} \cdot \tilde{m}_q - \frac{\tilde{v}_{sq}}{L} \tag{2.14}$$

As mentioned previously, the transition to the small signal model only resulted in a change of variables through this very simple derivation. This will also be the case for the other linear equations to be derived in this chapter. For compactness the simple transition to small signal model will not be explicitly shown for the other equations in this chapter, except for that in section 2.3.1. Also note that the tilde notation is generally dropped for simplicity and compactness throughout the rest of this thesis.

To briefly summarize this section, equation 2.13 and 2.14 constitute the small signal 2L-VLC model in the dq-reference frame. This is an averaged model that neglects any switching dynamics and imbalances in the three-phase system. It is coupled between the d- and q-axis which must be taken into account when designing the control system. However, it is a simple linear model that will reduce the complexity of the analysis and the computational time needed for computer simulations. It also avoids later complications by facilitating the use of conventional linear control theory in both modeling and analysis.

As a final comment it should be noted that the rotating dq-reference frame of the controller logic must be synchronized with the inherent reference frame of the physical system. This is commonly done by the use of a Phase-Locked Loop (PLL) scheme. The PLL implementation adopted in this thesis and how it influences the system is presented in section 2.3.1. Furthermore, the need for synchronization schemes such as the PLL is often considered a disadvantage of the dq-frame modeling.

2.3 Construction of Complete Converter Model and Stability Assessment Method

In this section the previously derived pieces will be combined with a control system into the complete converter model to be used in this thesis. Then the equivalent impedance model to be used for stability assessment will be derived.

The starting point of the modeling is the averaged model of the 2L-VSC and filter derived in the previous section. Equation 2.13 and 2.14 may be visualized in

block diagram form as shown in figure 2.7. Also note that the equations has been transformed into the Laplace-domain.

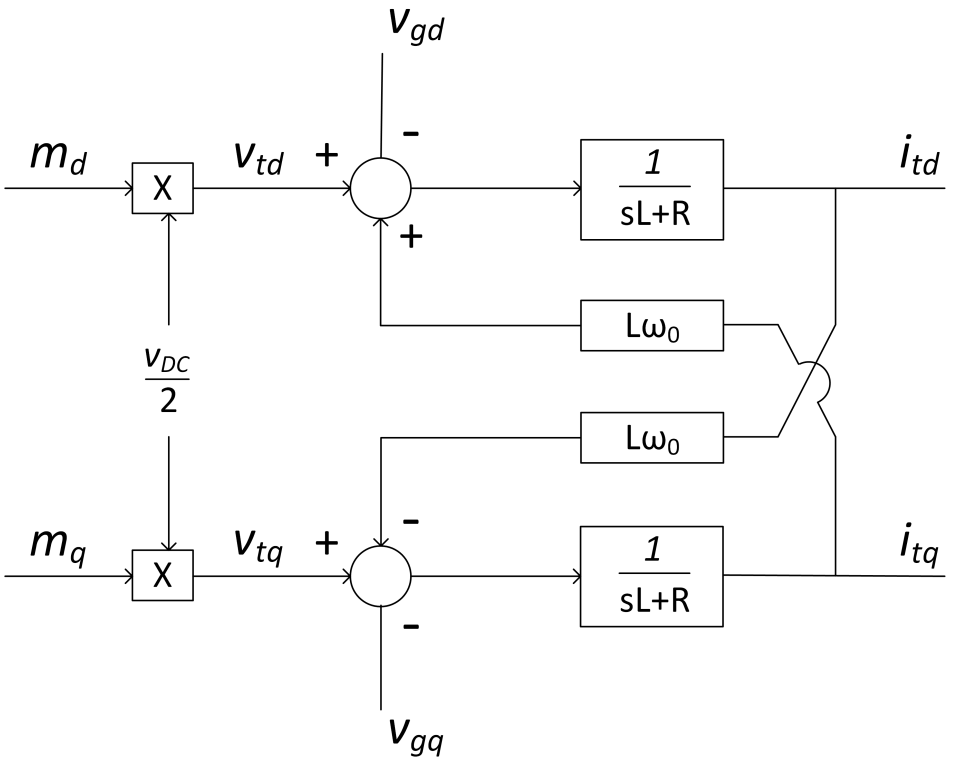

Figure 2.7: Visualization of equation 2.13 and 2.14 as a block diagram

As mentioned previously, one of the disadvantages of the dq-transformation is that equations are coupled. Thus, it would be difficult to regulate the d-axis current without affecting the q-axis current and vice versa, as is clearly visible from figure 2.7. This would complicate controller design to achieve proper operation. One possible solution to this problem is to introduce decoupling terms into the d- and q-axes [16]. This will ideally make the currents and voltages in the two axes independent of each other. The basic idea is to recognize that m_d and m_q are the output control signals of the converter and may thus be defined by convenience. That is, let u_d and u_q define two new control signals and let m_d and m_q be defined as in equations 2.15 and 2.16 respectively.

$$m_d = \frac{2}{V_{DC}} \cdot (u_d - L\omega_0 \cdot i_{tq} + v_{sd}) \tag{2.15}$$

$$m_q = \frac{2}{V_{DC}} \cdot (u_q + L\omega_0 \cdot i_{td} + v_{sq}) \tag{2.16}$$

Ideally this would make the d-axis current independent of both the q-axis current and the d-axis system voltage, as they would naturally be compensated by the addition of the terms into m_d. The same would apply to the q-axis current. This is visible from inspection of figure 2.9 below. Thus, in the ideal case, the d- and q-axis currents could be regulated by simple feedback and PI controllers to output the new control signals u_d and u_q as shown in figure 2.8.

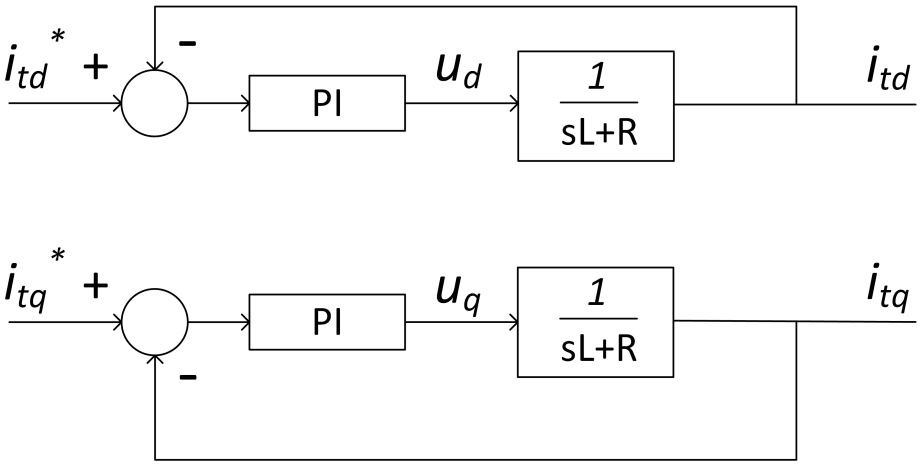

Figure 2.8: Equivalent converter control provided ideal decoupling

However, in actual systems the decoupling terms introduced in equation 2.15 and 2.16 would have to be measured and processed before they were sent into the controller. This would introduce delays, measurement noise, etc. into the compensating signals. Therefore, ideal decoupling as in figure 2.8 can not be expected. That is, the decoupling of the equations is an approximation whose validity should be considered as its performance will influence the performance of the control system. However, provided that the decoupling works sufficiently well, a simple PI controller can easily be used to regulate the current. The converter model including the decoupling terms of equations 2.15 and 2.16, PI controller, and measurement effects is shown in figure 2.9. For clarity, the sampling and possible measurement filters are marked in red color. Also note that the effect of the PWM scheme is included in the figure. The details of the modeling of measurement effects and PWM are presented in section 2.3.2. It should also be noted that in the general case the dc-voltage would also include some measurement effects, but as this is considered constant here, this is omitted. Additionally, the ω_0 term in the current decoupling would generally also be subject to some non-idealities in measurement or estimation. However, as the frequency deviations are included through the PLL

modeling in section 2.3.1, ω_0 will denote the actual system fundamental frequency also in the decoupling.

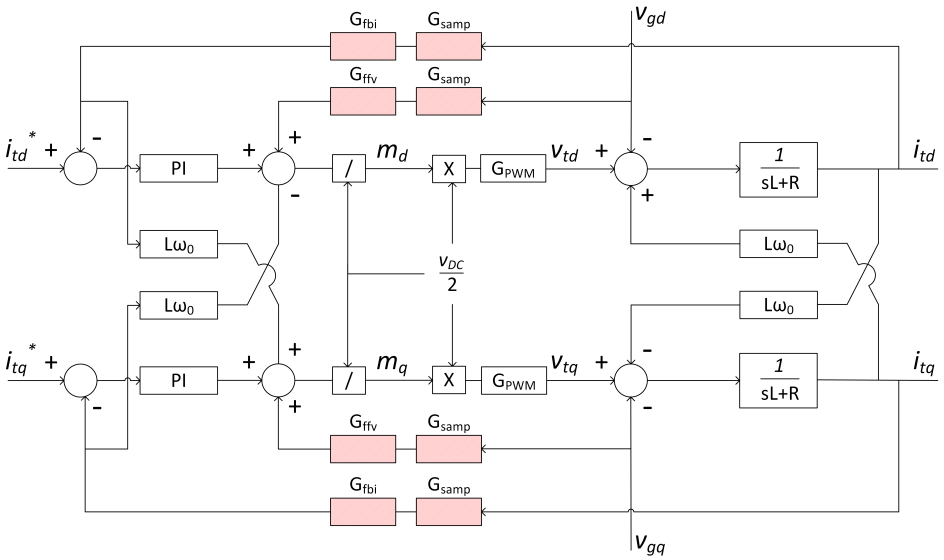

Figure 2.9: Converter model with current control, decoupling, and effects of measurements, sampling, and PWM included

For compactness, figure 2.9 will be transformed into a matrix equivalent. In all the following figures utilizing matrix form, the adopted convention is that all matrices and vectors will be indicated by bold letters. Furthermore, any vector input to a block will be right-multiplied with the block's content. The matrix form of figure 2.9 is shown in figure 2.10. Details on equations and matrices can be found in Appendix C.

In addition to the mentioned measurement effects, also the non-ideal effects of the grid synchronization should be taken into account. Details on this are described in section 2.3.1. As shown therein, the effect of the imperfect synchronization by the PLL can be modeled as the addition of the disturbance in q-axis voltage through the PLL transfer matrices into the three converter-system interfaces considered. That is, current- and voltage- measurements as well as the duty-ratio output.

This last addition of PLL effects is shown in figure 2.11, which will constitute the complete converter model to be used in this thesis. The PLL effects are shown in green color for clarity.

It should be noted that there are several other effects that could have been taken into account such as dc-side dynamics, effects of reactive power and other outer control loops, to mention a few. However, the previously mentioned effects are neglected in accordance with the scope stated in the introduction. For the purpose of

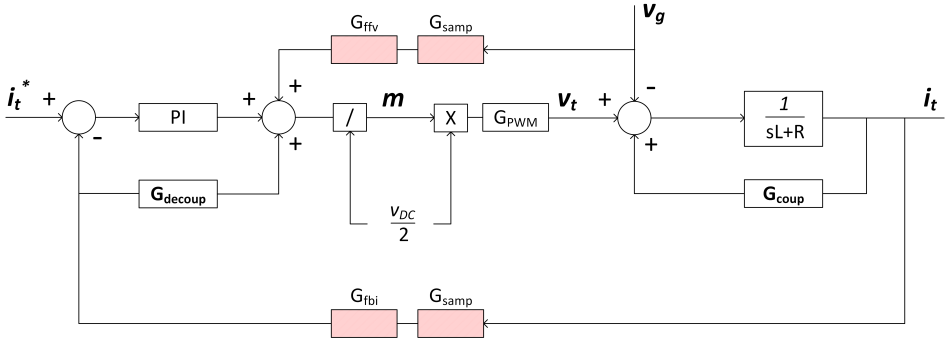

Figure 2.10: Matrix form of converter model with current control, decoupling, and effects of measurements, sampling, and PWM included

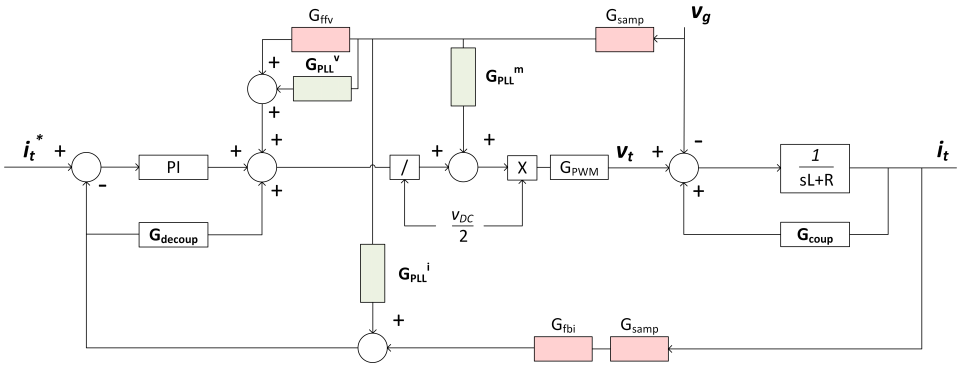

Figure 2.11: Complete converter model including current control, decoupling, effects of measurements, sampling, PWM, and PLL effects included

this thesis the presented model is considered sufficient and is kept simple to avoid unnecessary complications in later derivations. It should also be kept in mind the value of a simple model, as this would require less computational power from a PEC's processor. That is, if the simplified model were to show sufficiently accurate results it could be preferable as it would be quicker in the case of online implementation. Additionally requirements on the converter's processor would be kept to a minimum, in accordance with the guidelines presented in the introduction.

2.3.1 Phase-Locked Loop and Its Influence

This section will briefly explain how the PLL influences the converter model in this thesis. The theory in this section is based on what is reported in [18].

As mentioned briefly towards the end of section 2.2, the converter must be syn-

chronized to the grid to function properly. That is, to issue the correct command signals the dq-reference frame of the converter controller must be aligned with that of the native physical system. As is further explained in appendix A, the d-axis of the control system is intended to be aligned with the phasor of the system voltage. There are several alternative ways of achieving this, but the PLL is chosen in this thesis because of its widespread use.

The PLL can be implemented as shown in figure 2.12, where the transfer function H_{PLL} is that of the PLL's PI controller, and the abc/dq-block symbolizes the Park transformation in equation 2.9.

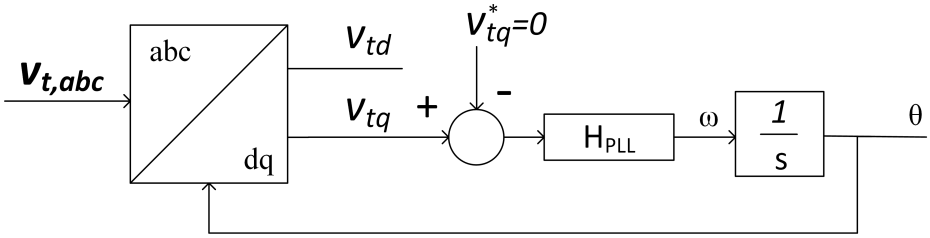

Figure 2.12: PLL block diagram

The PLL synchronizes the frequency of the converter to that of the system by regulating the angle used in the Park transformation, so that the q-axis voltage will match some reference value. Referring to Appendix A, driving the error between the measured and reference value to zero would ensure that the dq-frame would rotate at he same angular velocity as that of the system phasors. That is, the converter and system frequency would be equal. In this thesis, the q-axis terminal voltage reference is chosen to be zero as shown in figure 2.12. This would in turn make the desired angle between the dq-reference frame and the terminal voltage phasor equal to zero.

Unfortunately, the PLL will introduce additional dynamics into the converter operation that can have detrimental effects on the system stability. To understand the reason for this, consider the system under analysis as being composed of two dq-frame domains as in [18]. One domain is the inherent dq representation of the physical system, and the other is the dq-reference frame of the converter control system. Subsequent to some disturbance in the q-axis voltage, the reference frames in the two domains may not be perfectly synchronized because of the PLL controller dynamics. Therefore, a d-axis signal of the converter may not be perfectly translated into a d-axis signal in the physical system, and vice versa. The mapping of signals between the two domains can be done via the rotation matrix, $\mathbf{T}_\theta$, shown in equation 2.17 below

$$\mathbf{T}_\theta = \begin{bmatrix} \cos(\theta) & \sin(\theta) \\ -\sin(\theta) & \cos(\theta) \end{bmatrix} \tag{2.17}$$

where θ is the output angle of the PLL which also is the difference in angle between the two rotating reference frames.

Thus, for clarity and to indicate the ramifications, consider the following: If there is a disturbance in the source voltage, this will propagate to the control system through the output angle of the PLL. This will further affect the current controller as the measured values will be incorrectly translated. The affected control signals will then be issued to the PWM reference and will yet again be influenced by the erroneous transformation angle when the signals are translated from controller reference frame to the physical reference frame of the switches. Therefore, a disturbance in the q-axis voltage will propagate through the control system and cause the converter switches to be issued with distorted control signals, which in turn will cause the converter to output unintended currents and voltages [18].

Because of this, the PLL dynamics must be included in the modeling of the VSC to avoid neglecting important aspects to the system stability. The effects are modeled in accordance with [18] and the derivation is shown below.

In steady-state, the d and q values in the corresponding domains would be equal to each other. That is, $\mathbf{V}^c = \mathbf{V}^s$, where superscript c and s denotes controller reference frame and system reference frame respectively. This follows from the fact that the PI controller would eliminate any steady-state deviation in the angle, and thus the reference frame of the control system and physical system would be perfectly synchronized. This can be expressed by the rotational matrix in equation 2.17 as shown in equation 2.18

$$\mathbf{V}^c = \begin{bmatrix} \cos 0 & \sin 0 \\ -\sin 0 & \cos 0 \end{bmatrix} \cdot \mathbf{V}^s \tag{2.18}$$

where θ is regulated to zero as mentioned previously and explained in appendix A.

According to the small signal assumption, a small perturbation can be added to the relation in 2.18 as shown in equation 2.19 [18]

$$\begin{bmatrix} V_d^c + \tilde{v}_d^c \\ V_q^c + \tilde{v}_q^c \end{bmatrix} = \begin{bmatrix} \cos(0 + \tilde{\theta}) & \sin(0 + \tilde{\theta}) \\ -\sin(0 + \tilde{\theta}) & \cos(0 + \tilde{\theta}) \end{bmatrix} \cdot \begin{bmatrix} V_d^s + \tilde{v}_d^s \\ V_q^s + \tilde{v}_q^s \end{bmatrix} \tag{2.19}$$

where $\tilde{v}_d^c$, $\tilde{v}_q^c$, $\tilde{v}_d^s$, $\tilde{v}_q^s$ are small perturbations to the d and q component of the controller and system voltage respectively. $\tilde{\theta}$ denotes a small perturbation to the PLL output angle.

Equation 2.19 may be simplified by the use of trigonometric approximations and canceling the steady-state terms, which are assumed to be equal. This yields equation 2.20 and subsequently equation 2.21.

$$\begin{bmatrix} V_d^c + \tilde{v}_d^c \\ V_q^c + \tilde{v}_q^c \end{bmatrix} \approx \begin{bmatrix} 1 & \tilde{\theta} \\ -\tilde{\theta} & 1 \end{bmatrix} \cdot \begin{bmatrix} V_d^s + \tilde{v}_d^s \\ V_q^s + \tilde{v}_q^s \end{bmatrix} \tag{2.20}$$

$$\begin{bmatrix} \tilde{v}_d^c \\ \tilde{v}_q^c \end{bmatrix} \approx \begin{bmatrix} \tilde{v}_d^s + \tilde{\theta} \cdot V_q^s \\ \tilde{v}_q^s - \tilde{\theta} \cdot V_d^s \end{bmatrix} \tag{2.21}$$

The perturbation in the output angle of the PLL, $\tilde{\theta}$, is due to the perturbation in the q-axis voltage referred to the controller reference frame and the PLL controller dynamics. This may be written as in equation 2.22

$$\tilde{\theta} = \tilde{v}_q^c \cdot H_{PLL} \cdot \frac{1}{s} \tag{2.22}$$

where H_{PLL} is the transfer function of the PLL PI controller and possible low pass filter, while $\tilde{v}_q^c$ is the error signal shown in figure 2.12.

Substituting 2.22 into the second row of equation 2.21, and neglecting terms where two small disturbances are multiplied, yields the transfer function from a small perturbation in q-axis voltage to a response in PLL output angle. This is shown in equation 2.23.

$$\tilde{\theta} = \frac{H_{PLL}}{s + V_d^s \cdot H_{PLL}} \tilde{v}_q^s \tag{2.23}$$

Let the transfer function in equation 2.23 be denoted G_{PLL} as shown in equation 2.24.

$$G_{PLL} = \frac{H_{PLL}}{s + V_d^s \cdot H_{PLL}} \tag{2.24}$$

Similar derivations can be carried out to yield how a disturbance in the voltage propagates over the system-controller interfaces through the PLL [18]. That is, how the disturbance propagates into the modulating signal and current controller. The impact of a voltage disturbance on the current measurement is shown in equation 2.25 and the corresponding transfer matrix is defined in 2.26. The impact on the modulating signal is shown in equation 2.27 and a corresponding transfer matrix is defined in 2.28.

$$\begin{bmatrix} \tilde{i}_d^c \\ \tilde{i}_q^c \end{bmatrix} \approx \begin{bmatrix} 0 & I_q^s \cdot G_{PLL} \\ 0 & -I_d^s \cdot G_{PLL} \end{bmatrix} \cdot \begin{bmatrix} \tilde{v}_d^s \\ \tilde{v}_q^s \end{bmatrix} + \begin{bmatrix} \tilde{i}_d^s \\ \tilde{i}_q^s \end{bmatrix} \tag{2.25}$$

$$\mathbf{G}_{PLL}^i = \begin{bmatrix} 0 & I_q^s \cdot G_{PLL} \\ 0 & -I_d^s \cdot G_{PLL} \end{bmatrix} \tag{2.26}$$

$$\begin{bmatrix} \tilde{m}_d^c \\ \tilde{m}_q^c \end{bmatrix} \approx \begin{bmatrix} 0 & M_q^s \cdot G_{PLL} \\ 0 & -M_d^s \cdot G_{PLL} \end{bmatrix} \cdot \begin{bmatrix} \tilde{v}_d^s \\ \tilde{v}_q^s \end{bmatrix} + \begin{bmatrix} \tilde{m}_d^s \\ \tilde{m}_q^s \end{bmatrix} \tag{2.27}$$

Note here that the modulating signal is transferred from the controller domain to the system domain, i.e. opposite to what is shown in equation 2.27. Therefore, let the voltage disturbance to modulating signal response transfer function, $\mathbf{G}_{PLL}^m$, be defined as shown in equation 2.28.

$$\mathbf{G}_{PLL}^m = \begin{bmatrix} 0 & -M_q^s \cdot G_{PLL} \\ 0 & M_d^s \cdot G_{PLL} \end{bmatrix} \tag{2.28}$$

The voltage in equation 2.21 may, of course, also be brought on this form, shown below for completeness.

$$\begin{bmatrix} \tilde{v}_d^c \\ \tilde{v}_q^c \end{bmatrix} \approx \begin{bmatrix} 0 & V_d^s \cdot G_{PLL} \\ 0 & -V_q^s \cdot G_{PLL} \end{bmatrix} \cdot \begin{bmatrix} \tilde{v}_d^s \\ \tilde{v}_q^s \end{bmatrix} + \begin{bmatrix} \tilde{v}_d^s \\ \tilde{v}_q^s \end{bmatrix} \tag{2.29}$$

$$\mathbf{G}_{PLL}^v = \begin{bmatrix} 0 & V_d^s \cdot G_{PLL} \\ 0 & -V_q^s \cdot G_{PLL} \end{bmatrix} \tag{2.30}$$

From the above equations it is clear that the effect of the PLL can be modeled simply as a disturbance from the voltage added into the original signal through a transfer function or equivalent transfer matrix. Furthermore, note that equations 2.26, 2.28, and 2.30 are used directly in figure 2.11

2.3.2 Modeling of PWM and Sampling Effects

This section will briefly elaborate on the modeling choices behind the PWM and sampling effects.

As mentioned earlier, the applied model ignores any switching effects and high frequency dynamics. Therefore, the applied PWM scheme will not have much influence on the dynamics under study. However, one effect that will be included is the sample-and-hold effect in a digital PWM. Assume that the value of the modulating signal is sensed once per switching period (T_{sw}). Any change in the modulating signal within that period will not be sensed and updated until the consecutive switching period. This delay from command to actuation can take any value between 0 and one switching period T_{sw}. On average the delay is assumed to be one half switching period. Additionally, there will be some delay from converting an analogue signal to digital and back again. The entire process is assumed to take one switching period in total to complete. Because of this, the effect of the digital PWM implementation is modeled as a delay from command signal, $\mathbf{m}$, to actuation, $\frac{V_{DC}}{2}\mathbf{m}$, of 1.5 switching periods $1.5T_{sw}$ [14].

Likewise, any measurements of the voltages and currents will introduce delays in going from analogue to digital. It is also common to sample several times and use the average between these as the final measurement. Because of this it is assumed that any measurements would introduce a delay of $0.5T_{sw}$ [14].

The delays introduced by the PWM and measurement sampling could thus be represented in Laplace-domain as shown in equation 2.31 and 2.32 respectively.

$$G_{PWM} = e^{-1.5T_{sw} \cdot s} \tag{2.31}$$

$$G_{samp} = e^{-0.5T_{sw} \cdot s} \tag{2.32}$$

The above form, utilizing the exponential, could in some cases be quite inconvenient in the modeling. This can be avoided by approximating the delay by a second order Padé approximation shown in equation 2.33 below.

$$e^{-T \cdot s} \approx \frac{(T \cdot s)^2 - 6T \cdot s + 12}{(T \cdot s)^2 + 6T \cdot s + 12} \tag{2.33}$$

where T will be equal to $1.5T_{sw}$ and $0.5T_{sw}$ for the approximation of equation 2.31 and 2.32 respectively.

2.4 Stability Assessment

This section will elaborate on how the previously derived model can be used for stability assessment as well as deduce the required equations, and present the stability criterion.

In section 2.3, a linear approximate model of a 2L-VSC with constant dc-side voltage and corresponding current controller was derived. The complete model, in matrix form, is shown in figure 2.11. The next step is to convert this into a Norton equivalent to be used in the stability assessment, similar to that done in section 2.1. Some of the steps in this conversion are very laborious, and does not provide additional understanding of the stability criteria to be deduced. The explicit derivations of the Norton equivalent are therefore skipped to retain overview. Details on this can, however, be found in Appendix C. A compact account of this procedure is provided below.

By the use of linear control theory and the principle of superposition, an equivalent transfer matrix from the reference vector $\mathbf{I}_t^*$, to output current $\mathbf{I}_t$, can be found as shown in equation 2.34

$$\mathbf{I}_t = \mathbf{G}_{cl,i} \cdot \mathbf{I}_t^* \tag{2.34}$$

where $\mathbf{G_{cl,i}}$ denotes the closed loop current controller transfer matrix.

Similarly, the transfer matrix from terminal voltage to output current can be found as shown in equation 2.35

$$\mathbf{I_t} = -\mathbf{Y_o} \cdot \mathbf{V_t} \tag{2.35}$$

where $\mathbf{Y}_o$ denotes the equivalent converter output admittance matrix . Also note the minus sign in equation 2.35. This is introduced because the reference direction of the current is in the outward direction, i.e. out of the converter terminals. Therefore, an admittance behind these terminals would be the result of a negative current divided by the terminal voltage [19].

Equation 2.34 and 2.35 now constitutes the linear Norton equivalent of the PEC model. By combining this with a linear Thevenin equivalent model of the grid, a corresponding situation as that in figure 2.4 in section 2.1 can be obtained, although now in matrix form. This is shown in figure 2.13.

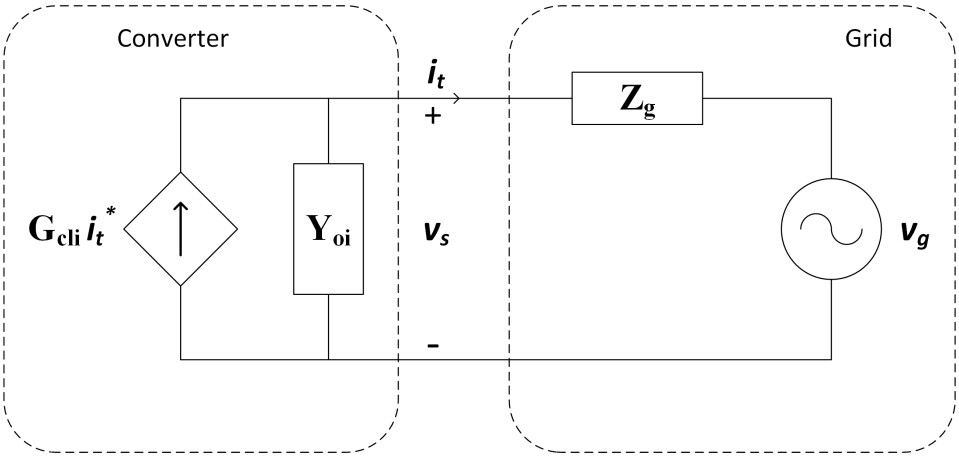

Figure 2.13: Small signal Norton equivalent connected to a Thevenin equivalent of the grid on matrix form

Note that figure 2.13 is identical to that in figure 2.4, except that all variables are vectors and all parameters are matrices here.

Similarly to section 2.1, the equivalent in figure 2.13 can be analyzed by linear circuit theory to yield the matrix equations 2.36 and 2.37.

$$\mathbf{I_t} = \mathbf{G_{cl,i}} \cdot \mathbf{I_t^*} - \mathbf{Y_o} \cdot \mathbf{V_t} \tag{2.36}$$

$$\mathbf{V_t} = \mathbf{Z_g} \cdot \mathbf{I_t} + \mathbf{V_s} \tag{2.37}$$

These can be combined into an equivalent block diagram shown in figure 2.14.

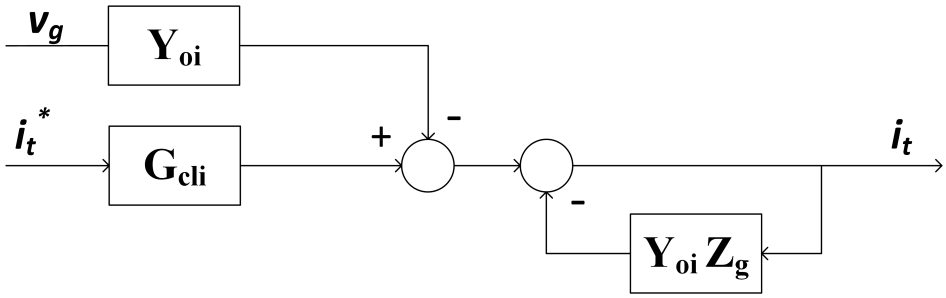

Figure 2.14: Block diagram of equations 2.36 and 2.37

In the same way as before, if the two terms on the left can be assumed to be stable, then the stability of the entire system will be determined by the minor loop gain given by equation 2.38.

$$\mathbf{G_{ml}}(s) = \mathbf{Y_o} \cdot \mathbf{Z_g} \tag{2.38}$$

The two terms $\mathbf{Y_o} \cdot \mathbf{V_s}$ and $\mathbf{G_{cl,i}} \cdot \mathbf{I_t^*}$ can be assumed to be stable also in the multivariable case. This does again translate into the current source being stable when unloaded, and the converter equivalent admittance being stable when supplied from an ideal grid [12]. This would most often be the case in actual systems, as it would be a prerequisite for connecting the converter in the first place.

The stability assessment in this section will involve a slight complication owing from the choice of the dq-system. The dq-model is a Multiple-Input-Multiple-Output (MIMO) system, as opposed to a simple Single-Input-Single-Output (SISO) system that would be the case if a per-phase- or certain sequence domain- systems were used [20]. For the SISO case, the traditional Nyquist criterion can be applied directly as outlined in section 2.1. However, for the MIMO case this Nyquist criterion would have to correspond to a generalized multivariable Nyquist criterion applied to the minor loop gain matrix [20, 21]. In this case the generalized Nyquist criterion translates into requiring the curves of the eigenvalues of the minor loop gain matrix to not encircle the point (-1,0) in the complex number plane [20, 21]. Also in the MIMO case the stability criterion is relatively simple compared to other methods, and may still be evaluated graphically to easily visualize the stability conditions of the system.

Yet another difference between the MIMO and the SISO case should be noted. Equation 2.36 and 2.37 can be combined in two different ways. Either by substituting for the terminal voltage, $\mathbf{V_t}$, which produces the above case, or to substitute for, $\mathbf{I_t}$, which would produce the block diagram in figure 2.15.

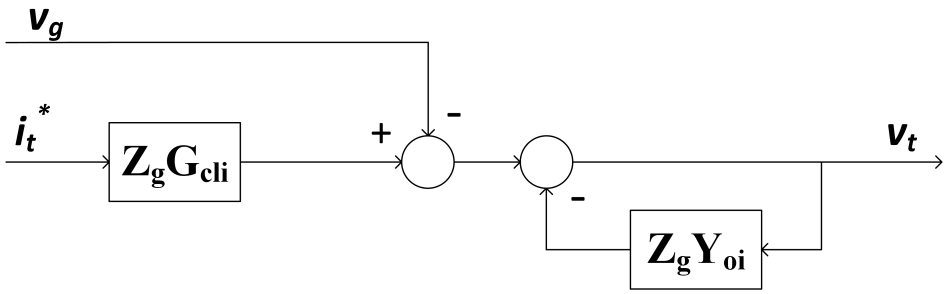

Figure 2.15: Alternative block diagram of equations 2.36 and 2.37

The minor loop gain would in the latter case be given by $\mathbf{Z_g} \cdot \mathbf{Y_o}$. In the SISO case, this would produce the same stability criterion. For the MIMO case, where the terms are matrices, the eigenvalues could be different for the two configurations as the order of the terms would matter. If the system was ideal, the decoupling terms and no interference from the PLL would make the converter admittance matrix $\mathbf{Y_o}$ diagonal. The two minor loop gains would thus yield the same eigenvalues. However, because of the sampling effects in measurements for the decoupling and the effect of the PLL this would not be exactly true. One could therefore think that both criteria should be checked. However, as pointed out in [12], because of the underlying assumptions of the model, the Norton and Thevenin equivalents may not be used interchangeably in this case. Based on this consideration it is concluded that only the analysis of the matrix $\mathbf{Y_o} \cdot \mathbf{Z_g}$ will yield the correct results

From the discussion presented in this section, it may be observed that the stability of the system, with regards to resonance, can be determined by the eigenvalues of the equivalent converter admittance and the equivalent grid impedance. The former will be known by the designer, and thus the only unknown will be the equivalent grid impedance. To be able to carry out the stability assessment, the unknown grid impedance must be estimated. This will be the topic of the next chapter.

Chapter 3

Grid Impedance Estimation

This chapter will clarify how the grid impedance can be estimated. First, the requirements for the estimation method are briefly elaborated. Afterwards, several methods are briefly presented to give an overview of some of the the possibilities, their main pros and cons, and the fact that a combination of methods often can be advantageous. One of the methods is then selected based on the considerations and guidelines of this thesis. Finally, the main theory and key considerations of the chosen method are explained together with some of the implementation choices made in this thesis.

3.1 Selection Criteria

The selection criteria for the grid impedance estimation method follows from the guidelines set forth in the introduction. Based on this, the following considerations are made.

Any method which require detailed modeling of the surrounding grid or strong assumptions of its contents and/or composition, are disqualified for use in this thesis. This is because such details are most often not readily available. Such detailed models will furthermore require considerable amounts of computational power, increasing time consumption and/or costs. Furthermore, as explained in the introduction, a desired property of the stability assessment method is the possibility to install a generic converter with minimal a priori knowledge of the surrounding system. This does in turn favour non-parametric estimation approaches.

Additionally, the grid impedance is exhibiting considerable variations over the course of a day and within single hours [11]. The grid impedance estimates should thus be regularly updated to capture these variations. In the case of an islanding event, the equivalent 'grid' impedance could furthermore change drastically

in a very short period of time. If the converter is intended to continue operation as a part of a microgrid, its stability could be severely challenged if the grid impedance estimates are not updated quickly enough. Also, in islanded operation, some or all present converters would have to switch from current controlled, to voltage controlled mode. In this mode of operation, the stability criterion with regard to grid impedance would be quite the opposite than that of the current controlled mode [12]. Therefore, switching to voltage controlled mode before the grid impedance estimate is updated and control parameters can be adjusted, could provoke instability. Lastly, grid impedance estimates could be used for island detection, which would put even stronger constraints on update time. Based on the above discussion, evaluation time will be considered a key parameter in the selection of grid impedance estimation method. It should be noted that the actual time-optimization of the chosen method is considered to be beyond the scope of this thesis. These considerations and selection criteria are nevertheless included here to allow such optimization to be carried out, and yield a sufficiently fast online estimation scheme in a further work.

In addition to time, it is considered important that the estimation should be implementable without the need for considerable upgrades of a generic PEC. Neither in hardware or processing power. This is to avoid additional costs which would reduce the competitiveness of RES as mentioned in the introduction.

There are several possible estimation methods available, and they can generally be divided into two kinds: Active and passive methods. There is also a possible extension of a third kind called quasi-passive methods, that is a hybrid of the two former. This framework will be used to classify the different approaches below. It is also worth noting that although different in approach, most estimation methods utilize the basic notion that any disturbance in for example the current, will give a corresponding response in the voltage proportional to the equivalent impedance between those terminals. That is, the definition of the small signal impedance [20]. This is of course provided that the signals remain within the linear region in accordance with the small signal assumption.

3.1.1 Passive Methods

Passive methods are methods in which disturbances already present in the system current- and voltage-waveforms, are utilized to estimate the grid impedance. These methods are as such non-intrusive to the grid. This is an advantage in systems with strict power quality requirements.

There are several different examples of passive methods, one of which is presented in [22]. This method utilizes a grid model which takes a measured voltage perturbation, and outputs an expected current. The error between the current estimate and measured current is then used to update the model parameters. However, even though this approach is reported to yield accurate results, it is disqualified from further consideration as it requires strong assumptions about the composition of

the grid. Another possible approach reported in [23] is to construct a set of linear equations from the measurements of consecutive operating points. Regression is then used to yield a single estimate of the equivalent grid impedance. The computational time for the regressions are reported to take less than 20μs and the entire entire method to take less than 0.2s. This could make it a candidate for the type of scheme considered in this thesis.

However, in relation to passive methods, some important notes should be made. These methods have been found to be ineffective under conditions where the repetition rate of the disturbances is not high enough or that the disturbances are not strong enough to be properly measured [22, 24, 25]. As such low disturbance conditions most often are the preferred operating mode of the grid, the passive methods are severely challenged. Because of this, they are disqualified from use alone in this thesis. The passive methods are nevertheless included here as they could be part of a quasi-passive scheme. The advantages and inclusion of the latter will become clear towards the end of this chapter.

3.1.2 Active Methods

Active methods are methods where signals are actively injected into the grid to perturb the system. The response is then captured and analyzed.

One example is the well known sinusoidal sweep, where sinusoidal signals are injected for each frequency of interest [11, 26]. This approach is often considered to be the most accurate of the ones considered in this thesis [24]. However, as the evaluation time can be in the range of several minutes [27], it is considered to be too time consuming for the use intended here.

Another possibility is to inject a single pulse perturbation as was done in [28]. The main idea is to simultaneously excite a wide frequency spectrum with the single pulse. This would in turn greatly reduce the required data acquisition time of the estimation method. In [28], the data acquisition was reported to be done in 23ms, while the complete estimates were ready in 27ms. This makes the pulse method the fastest estimation method to be considered in this thesis. However, there are some drawbacks that must be taken into account. One of which is that the accuracy of the method is limited by the energy distribution of the signal, which is largely uncontrollable [24]. Furthermore, to achieve a sufficient signal-to-noise ratio, the amplitude of the injected current pulse must often be quite large [24]. This is especially true in strong grid conditions, which would lead to increased stress on components and even the risk of exceeding component operating limits. Additionally, this latter risk of exceeding component limits is further increased if several converters utilizing this method are present in the same grid. This is because two or more converters could incidentally inject pulses at the same time, causing exceedingly high current spikes. This challenge would have to be overcome before the pulse injection method could be implemented for commonly available converters.

The last method to be considered for use in this thesis is the Maximum Length Binary Sequence (MLBS) [24, 27, 29]. This method builds on the same principle as that of the pulse method, where impulse signals are injected to estimate the grid impedance. However, the MLBS rather injects a sequence of pulses to yield the desired response. This facilitates the use of lower amplitude of the pulses which will make it less intrusive to the grid. The MLBS is furthermore deterministic so the injections can be repeated and averaged to remove noise. This will in turn further decrease the required amplitude of the injected signal. As it is a sequence of multiple pulses the MLBS will inevitably be more time consuming than a pure one-pulse method. However, the MLBS is still quite efficient with regard to time use. In one approach not optimized for time use the method is reported to require less than two seconds to yield and estimate [27].

3.1.3 Comparison and Selection

Based on the above discussion it may be concluded that from the methods considered, only the pulse method and MLBS are suited for the use intended in this thesis. That is, they exhibit potential for low time use and sufficient accuracy. The others are disqualified, except for the passive method utilizing a set of linear equations, but this would have to be implemented as part of a quasi-passive approach.

Both the MLBS and the pulse method have its own pros and cons. The main advantage of the pulse method is the short evaluation time, while that of the MLBS is its low intrusion level. However, when comparing these two, especially one distinguishing feature must be noted. This is the fact that under strong grid conditions and tight voltage restrictions, the pulse method has been shown to fail while the MLBS still performs acceptably [24]. This can be seen by referring to figures 3.1, 3.2a and 3.2b. In figure 3.1, the accuracy of the two methods are compared with an injection-amplitude restriction of 0.1 p.u. and strong grid conditions. The difference in the accuracy of the grid impedance estimate is clearly visible, with the MLBS yielding superior results. Moreover, in order to achieve similar accuracy as that of the MLBS, with injection amplitude restricted to 0.1 p.u., the pulse method would have to utilize a pulse amplitude of 1.5 p.u. The considerable difference in intrusion level for these two cases is clearly visible in figure 3.2a and 3.2b.

Furthermore, it is considered more likely that the MLBS will be able to achieve acceptable evaluation times through mathematical and computational optimization than the pulse injection method to overcome the inherent problems of high intrusion levels. Based on this, and the above discussion, the MLBS is chosen as the preferred grid impedance estimation method for the applications considered herein.

Lastly it should be noted that, the pulse method is not the only method that can possibly fail if several units were to inject perturbation signals at the same time. This is also true for the MLBS [11]. That is, if several MLBS' were injected at the same time, component ratings would probably not be exceeded because of low

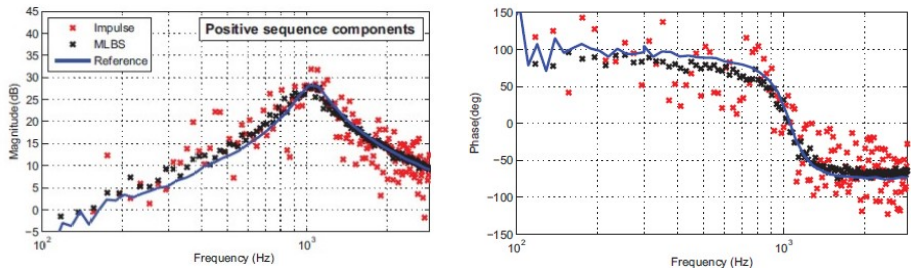

(a) Magnitude (b) Phase

Figure 3.1: The difference in accuracy for pulse injection and MLBS restricted to 0.1 p.u. injection amplitude. Reproduced from [24]

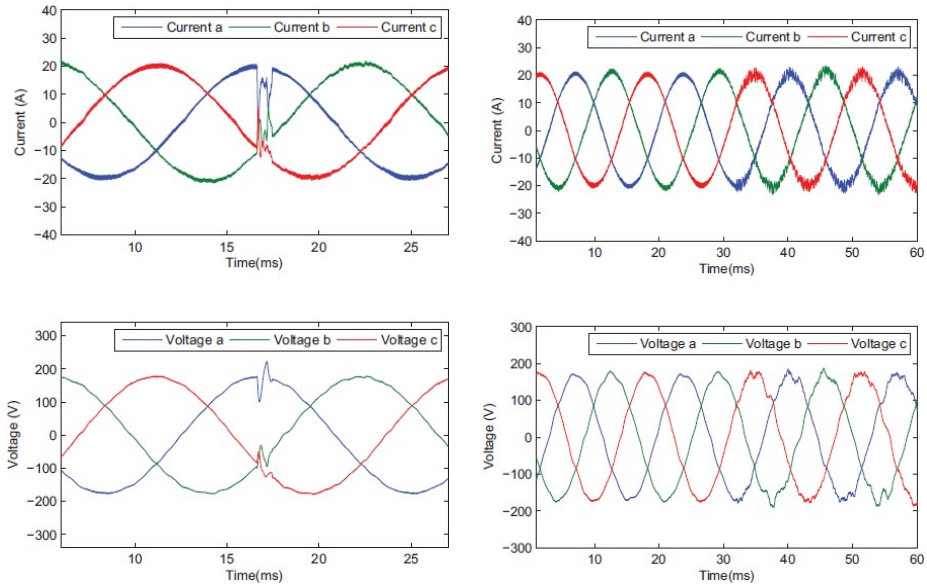

(a) Pulse Injection Method applying a pulse amplitude of 1,5 p.u.

(b) MLBS applying an injection amplitude of 0.1 p.u.

Figure 3.2: Degradation of current and voltage waveforms by the Pulse Injection Method and MLBS to achieve similar accuracy. Reproduced from [24]

amplitudes. However, the estimation method could yield unreliable results. This would thus also be a challenge if several converters were utilizing the MLBS in the same grid. One possible solution could be to implement the active method in conjunction with a passive method into a quasi-passive approach as mentioned above. In such a case, the converter would utilize the passive method and remain non-intrusive until the disturbances in the grid, and thus accuracy of the estimates, would drop below some threshold. Subsequently, the MLBS would be utilized to

perturb the system and estimate the grid impedance until the natural disturbances present in the grid again were strong enough to yield sufficient accuracy of the passive method. Because of time constraints and the fact that it is not an integral part of the main goals, this combination of an active and passive method into a quasi passive approach, is not implemented in this thesis. The above discussion is nevertheless included as these considerations would be an important part of a real life implementation, and are furthermore useful in assessing the applicability of the stability assessment method itself.

3.2 Maximum Length Binary Sequence

This section will expand on the key theoretical features of the MLBS, and also some of the practical considerations made for the implementation in this thesis.

3.2.1 Defining Features

The MLBS is part of a lager group of sequences called Pseudo Random Binary Sequences (PRBS). The PRBS have several defining features that should be taken into account. As the name implies, the sequences are binary, yielding outputs of 1 and 0. The outputs are subsequently mapped to appropriate amplitude levels before being injected into a system. Within one complete sequence there is *(P+1)/2* instances where the signal is at one level, and *(P-1)/2* where it is at the other. P denotes the sequence length here. If the binary signals are mapped to amplitude levels that are symmetrical about zero, the sequence average output will be close to zero. This will in turn reduce the intrusion level of the injected sequence. The PRBS are also intended to emulate white noise. That is, to cause simultaneous excitation of equal magnitude over a wide spectral range. This will in turn give a high signal-to-noise ratio (SNR) and simplify post processing [29].

The MLBS it will specifically have a sequence length given by $P = 2^n - 1$, where n is an integer. Additionally, each binary number in the sequence will appear exactly once before the sequence will start repeating itself [30]. The MLBS can also be predetermined so the injections can be repeated. This facilitates averaging over several injection periods to reduce the effect of background noise in the estimates. One of the great advantages of the MLBS is furthermore that the sequence can be easily generated by the use of a shift-register and XOR feedback. There is thus no need for elaborate techniques to generate the correct sequence. Further details on this can be found in appendix D.

3.2.2 Signal Design

By analyzing the energy in the MLBS, it can be determined that the signal will have no energy at the generation frequency, f_{gen}, and its multiples [30]. The MLBS can

actually only contain power at harmonically related cyclic frequencies[30]. That is, if the period of the sequence is denoted T, and the duration of a single binary pulse is denoted Δt_b, the MLBS will only contain power at frequencies given by equation 3.1.

$$f = \frac{k}{T} = \frac{k}{N \cdot \Delta t_b} = \frac{k}{N} \cdot f_{gen} \tag{3.1}$$

The power spectrum of the MLBS can then be written as in equation 3.2,

$$\Phi_{MLBS}\left(f = \frac{k}{T}\right) = \frac{a^2(P+1)}{P^2} \cdot \frac{\sin^2\left(\frac{\pi k}{P}\right)}{\left(\frac{\pi k}{P}\right)^2},\ k = \pm 1, \pm 2, ... \tag{3.2}$$

where k is an integer often referred to as the spectral line number [30].

As mentioned previously, the MLBS is intended to emulate white noise and thus to excite equal energies over a wide spectral range. The energy of the MLBS is obviously not flat as was assumed above, however it is often considered to be so until the power has dropped by 3dB [24]. The frequency at this point is approximately 0.45 f_{gen}, where f_{gen} denotes the generation frequency of the sequence. 0.45 f_{gen} will often be regarded as the limit for accuracy, and f_{gen} should thus be chosen to make all frequencies of interest fall within this this frequency band. It should also be noted that the harmonic spacing of the spectral energy lines is given by the ratio between the switching frequency and the generation frequency f_{gen}/P. Referring to equation 3.2, increasing P while keeping f_{gen} constant will give more spectral lines, or higher frequency resolution. However, this will also reduce the energy of each line.

The frequencies of equation 3.1 that contain power can be rewritten to yield equation 3.3

$$f_i = i \cdot \frac{f_{gen}}{2^n - 1},\ i = 1, 2, ..., P - 1 \tag{3.3}$$

where n is the degree of the shift register, i is an integer and f_{gen} is the perturbation generation frequency as before [27].

The MLBS will give leakage free response results, if there are no other major frequencies beyond those in equation 3.3 that affect the system to be tested. However, the power grid will inevitably have a 50Hz component that will affect the system, and this may cause leakage [27]. Thus, if this leakage is to be avoided, a constraint must be placed on the choice of generating frequency, f_{gen}, such that one of its harmonics must lie at the fundamental frequency of the system [27]. That is, equation 3.4 must be satisfied for some integer $i \in [1, 2, ..., P - 1]$

$$50 = i \cdot \frac{f_{gen}}{2^n - 1} \tag{3.4}$$

Many practical systems will still contain non-idealities and noise that may cause leakage. Therefore, it may still be necessary with measures such as spectral averaging, windowing functions etc.

Another constraint is placed on either the choice of generation frequency, or the switching frequency of the converter, by the effect of the PWM. As shown in [31] and pointed out in [27], the modulation generates several aliases in the response when an excitation signal is fed through the PWM and into the system. The perturbation responses will be caused at frequencies $k \cdot f_{sw} \pm f_m$, where f_m is the frequency of the intended excitation signal, k is some integer, and f_{sw} is the switching frequency of the converter. The lowest aliased frequency will also tend to be the one producing the largest perturbation response. Any frequency above $f_{sw}/2$ should therefore be filtered from the excitation to avoid aliasing [27].

The measurement results will also suffer from time aliasing if the excitation period is not equal to or larger than the settling time of the systems impulse response T_{imp}, as shown by [32]. Therefore, the signal length P should be selected to satisfy this criterion. However, as pointed out in [24], the settling time for the grid voltages and currents for small perturbations are usually a fraction of a fundamental cycle, while practical sequence injections are typically close to a fundamental cycle. In such a case, the time aliasing will not be an issue and the period length could be chosen more freely.

As mentioned previously, the MLBS is deterministic and may be averaged to reduce noise. The noise will be reduced by $1/\sqrt{R}$, where R is the number of injection periods [24]. The choice of R will depend on the desired accuracy, time requirements and possibly memory constraints in the converter, which may vary from case to case.

The last parameter to be explored is the injection signal amplitude. This must be chosen low enough to avoid exceeding limits and exciting non-linear responses, but still high enough to give sufficient SNR within the existing constraints. This could vary from one case to another, which makes it difficult to give general statements of how to design it. Therefore, this will be set on the basis of testing and heuristics in this thesis.

3.2.3 dq-Modeling Considerations

There is an important point that must be noted when discussing the grid impedance estimation in a dq-modeled system. In the dq-modeling, the impedance will be a 2x2 matrix containing four elements. In order to determine the value of these elements, the results of two linearly independent injections must be combined, as opposed to for instance a single phase system [20]. There are several ways of ensuring this. One of which is to let one injected signal be a pure d-axis component, while the other is a pure q-axis component. These two signals will then be orthogonal in the dq-domain ensuring linear independence, and may additionally lead to improved accuracy in experiments [20]. Some of the drawbacks of this approach

is that it requires a fast PLL to keep the controller axes synchronized to the grid voltage, and that the PLL dynamics may interfere with the measurement results [20]. This will also make the grid impedance estimation slower as two separate full MLBS' must be injected. However, as time optimization is outside the scope of this thesis and as injecting the signals in different axes will simplify the implementation, the above method is adopted in this thesis.

3.2.4 Post Processing

After the injected signal has perturbed the system and the response has been captured, the measurements will have to be processed to yield the equivalent grid impedance. The Fast Fourier Transform (FFT) is applied to the captured data to yield the corresponding frequency components of both voltage and current. For each frequency there will be four captured components of the current, and four of the voltage, as shown in equation 3.5 and 3.6 respectively.

$$\mathbf{I}_t = \begin{bmatrix} i_{dd} & i_{dq} \\ i_{qd} & i_{qq} \end{bmatrix} \tag{3.5}$$

$$\mathbf{V}_t = \begin{bmatrix} v_{dd} & v_{dq} \\ v_{qd} & v_{qq} \end{bmatrix} \tag{3.6}$$

In equation 3.5, i_{dd} is the captured d-axis current when the d-axis is injected with the MLBS, i_{dq} is the captured d-axis current when the q-axis is injected with the MLBS and so forth. The same nomenclature applies for the voltages in equation 3.6. From its definition, the small signal impedance for each frequency can thus be computed as shown in equation 3.7.

$$\mathbf{Z}_g = \begin{bmatrix} Z_{dd} & Z_{dq} \\ Z_{qd} & Z_{qq} \end{bmatrix} = \begin{bmatrix} v_{dd} & v_{dq} \\ v_{qd} & v_{qq} \end{bmatrix} \cdot \begin{bmatrix} i_{dd} & i_{dq} \\ i_{qd} & i_{qq} \end{bmatrix}^{-1} \tag{3.7}$$

If computed successfully, the above impedance could be used in the stability criterion of section 2.4, and the system stability could be assessed.

However, also in this case there are several notes that should be made. The analyzed interval of data used in the FFT should be an integer number of fundamental frequency periods. If not, the fundamental frequency components will cause spectral leakage [20]. In this regard there is also a further complication, namely that in real systems the grid frequency will vary over time. Therefore, the recorded time interval may not accurately fit to multiples of the fundamental frequency. This can lead to errors, not only due to the mentioned spectral leakage, but also due to artificial phase shifts caused by the fundamental frequency mismatch [33]. As in the signal design above, also this practical effect calls for additional measures. Possible remedies could be the use of window functions, digital filters, or sampling rate

adjustment [33]. Another consideration to be made is that the sampling frequency must be selected to be at least double that of the largest frequency component of interest to avoid aliasing.

Chapter 4

Adaptive Control

At this point, both an analytical model of the converter admittance, as well a method for estimating the grid impedance have been established. The stability of the converter can thus be analyzed. There would also be an obvious gain in not only assessing the stability, but also to re-tune the converter control parameters to avoid potential instabilities. In this section, a simple adaptive control is proposed to improve the stability of the converter based on the results of the stability assessment.

As was explained in section 2.4, the stability of the system with regards to resonance is determined by the eigenvalues of the minor loop gain $\mathbf{Y_o} \cdot \mathbf{Z_g}$. Graphically, this means that the plotted curves of the eigenvalues may not encircle the point (-1,0) in the complex number plane. As $\mathbf{Y_o} \cdot \mathbf{Z_g}$ is a two by two matrix, two eigenvalues will generally exist. Let these two eigenvalues be denoted λ_1 and λ_2. Furthermore, note that λ_1 and λ_2 will be functions of an angular frequency that traverses from negative infinity to positive infinity, in the same way as for Nyquist plots.

Consider figure 4.1, which depicts an example of the shape of the eigenvalue curves resulting from the analytical model will take. Also note that for the model deduced in this thesis, the eigenvalue curves will generally take this shape, although they will approach the (-1,0) point for larger values of the grid inductance. One of the eigenvalue curves is plotted in blue while the other is plotted in red. There will be a point on either λ_1 or λ_2 where the distance, $\mathcal{D}$, to the point (-1,0) is minimal. If it is assumed that λ_1 and λ_2 are not initially encircling the point (-1,0), the minimal distance $\mathcal{D}$ could be considered to be a measure of stability. That is, the smaller the value of $\mathcal{D}$, the closer the system would be to instability. This simple idea will form the basis of the adaptive control scheme presented in this chapter.

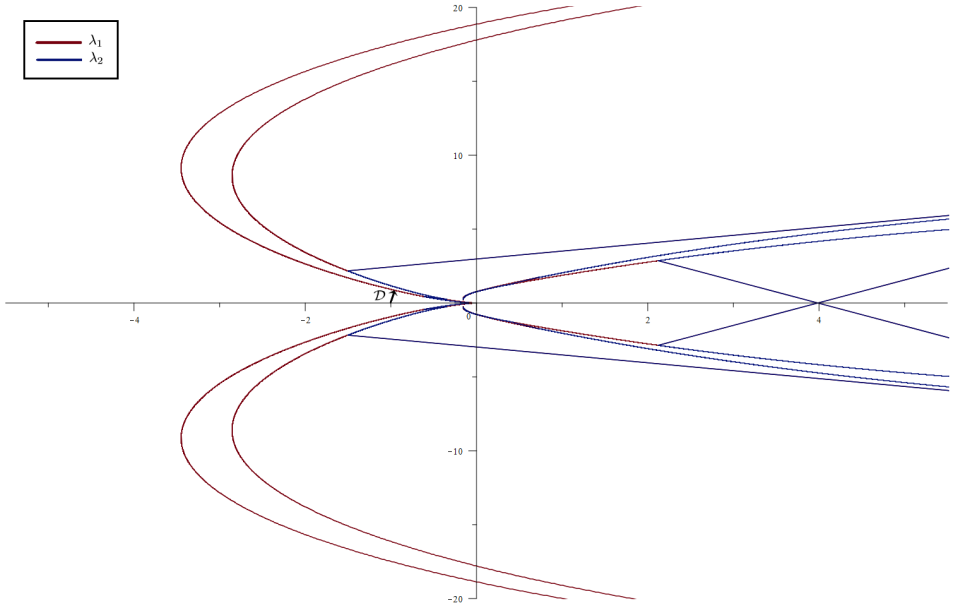

Figure 4.1: Eigenvalue curves created from actual analytical model

4.1 Determining the Stability Measure $\mathcal{D}$ and Initial Condition

The eigenvalue plots may be described in a more convenient way by considering the following. Let a new cartesian axis system be defined to have its axes oriented in the same way as the original complex number plane, but with its origin in the point (-1,0). Then λ_1 and λ_2 could be described as two parametrized curves given by the vectors shown in equation 4.1 and 4.2.

$$\vec{r_1}(\omega) = [1 + \mathrm{Re}(\lambda_1(\omega)), \mathrm{Im}(\lambda_1(\omega))] \tag{4.1}$$

$$\vec{r_2}(\omega) = [1 + \mathrm{Re}(\lambda_2(\omega)), \mathrm{Im}(\lambda_2(\omega))] \tag{4.2}$$

where the frequency ω is the parameter, and Re and Im respectively denote the real part and imaginary part of the function. Again, as the angular frequency traverses from negative infinity to positive infinity, ω is defined as $-\infty < \omega < \infty$.

By utilizing this form, the distance from the point (-1,0) to a point on one of the two curves, is simply given by the length of the respective vector $\vec{r}(\omega)$. Or as shown in equation 4.3.

$$R(\omega) = |\vec{r}(\omega)| = \sqrt{(1 + \mathrm{Re}(\lambda(\omega)))^2 + (\mathrm{Im}(\lambda(\omega)))^2} \tag{4.3}$$

The frequency that gives the minimum distance can be found by simply analyzing the equation 4.4 for each of the two curves.

$$\frac{dR(\omega)}{d\omega} = 0 \tag{4.4}$$

The minimum distance $\mathcal{D}$ from the point (-1,0) to one of the two curves λ_1 or λ_2, could thus ideally be determined in a simple manner.

It should be noted that the parameter $\mathcal{D}$ does not yield any information on whether the eigenvalue curves encircle the point (-1,0) or not. However, if the converter initially is stable, $\mathcal{D}$ would decay towards zero before it would start rising again after the eigenvalue curve crossed over the (-1,0) point. This crossing into instability could thus be detected. The adaptive controller would also naturally need to keep $\mathcal{D}$ above some threshold to account for inaccuracies in measurements and models. If $\mathcal{D}$ were to move beyond this threshold, it would mean that the adaptive control had expended its influence. Therefore, if $\mathcal{D}$ crossed over and started to rise it would be of little consequence, as the adaptive control would be out of options and the converter would have tipped into instability. Nevertheless, it would also be possible to easily check whether or not (-1,0) is inside or outside an eigenvalue curve. If the the parametrized curves 4.1 and 4.2 in the new cartesian coordinate system are converted to polar coordinates, the change in angle as the curve was traversed could be determined. If the absolute value of the net change in angle is less than 2π, then the curves λ_1 or λ_2 will not encircle the point (-1,0).

4.2 Parameter Tuning

The aim of the adaptive controller is to manipulate the accessible converter parameters in order to alter the equivalent converter admittance matrix $\mathbf{Y_o}$. This will in turn reshape the eigenvalue curves λ_1 and/or λ_2, and alter the distance $\mathcal{D}$. This is done to maintain $\mathcal{D}$ above some predefined threshold. From section 2.3 or appendix C, it can be seen that there are four controller parameters that may be manipulated, namely the current controller proportional and integral gains, and the PLL proportional and integral gains. Additionally, in extreme cases, it could perhaps be considered appropriate to manipulate the current references as a last resort to maintain stability.

The adaptive control may be exercised in several ways, but one simple approach is gain-scheduling. This is also the approach that will be adopted here. That is, the mentioned current controller and PLL gains, will be altered directly to achieve the desired result.

In the next sections, two possible ways of implementing the adaptive control scheme based on gain-scheduling will be elaborated.

4.3 Analytical Expression

One possible approach to the adaptive control, is to develop an analytical expression for the distance $\mathcal{D}$. The effect of a change in one of the parameters on the distance $\mathcal{D}$ can then be determined from the partial derivative of $\mathcal{D}$ with respect to that parameter. From the short discussion in section 4.1, this could seem to be straightforward. However, there are some complications that must be taken into account.

Consider the minor loop gain $\mathbf{Y_o} \cdot \mathbf{Z_g}$ shown in equation 4.5

$$\mathbf{G}_{ML} = \mathbf{Y_o} \cdot \mathbf{Z_g} = \begin{bmatrix} g_1 & g_2 \\ g_3 & g_4 \end{bmatrix} \tag{4.5}$$

The eigenvalues of this matrix can be found by solving equation 4.6

$$|\mathbf{G}_{ML} - \lambda \cdot \mathbf{I}| = \begin{vmatrix} g_1 - \lambda & g_2 \\ g_3 & g_4 - \lambda \end{vmatrix} = 0 \tag{4.6}$$

which will yield the second order polynomial shown in equation 4.7

$$\lambda^2 - k\lambda + l = 0 \tag{4.7}$$

where k denotes $g_1 + g_4$ and l denotes $g_1 \cdot g_4 - g_2 \cdot g_3$.

Equation 4.7 will generally have two solutions λ_1 and λ_2, shown in equations 4.8 and 4.9

$$\lambda_1 = \frac{k + \sqrt{k^2 - 4l}}{2} \tag{4.8}$$

$$\lambda_2 = \frac{k - \sqrt{k^2 - 4l}}{2} \tag{4.9}$$

It should be noted that as the minor loop gain matrix is based from circuit equivalents and grid parameters, λ_1 and λ_2, and in particular k and l, will contain both real and complex components. This causes some problems because, to develop an analytical expression of the distance R in equation 4.3, would require to split λ into a real and complex part. Splitting equations 4.8 and 4.9 into a real and complex part is not trivial, because of the complex values under the square root term.

One possible way to overcome this is to consider the following result from classical mathematics:

Let a, b, u, and $\mathbf{v}$ be real numbers. If the square root of $a + ib$ can be written as $u + iv$, as shown in equation 4.10,

$$\sqrt{a + ib} = u + iv \tag{4.10}$$

then

$$a + ib = (u + iv)^2 = (u^2 - v^2) + i \cdot 2 \cdot u \cdot v \tag{4.11}$$

Thus u and v will fulfill equations 4.12 and 4.13.

$$u^2 - v^2 = a \tag{4.12}$$

$$2u \cdot v = b \tag{4.13}$$

Or equivalently, equation 4.14 and 4.15.

$$u^2 = a + v^2 \tag{4.14}$$

$$4u^2 \cdot v^2 = b^2 \tag{4.15}$$

Combining 4.14 and 4.15 yields

$$4(a + v^2) \cdot v^2 = b^2 \tag{4.16}$$

or

$$(v^2)^2 + a \cdot v^2 - \frac{b^2}{4} = 0 \tag{4.17}$$

Equation 4.17 is a second order polynomial in v^2 that will have solutions shown in equation 4.18.

$$v^2 = -\frac{a}{2} \pm \frac{1}{2} \cdot \sqrt{a^2 + b^2} \tag{4.18}$$

Since $v^2 \geq 0$, equation 4.18 is equal to equation 4.19.

$$v = \pm\sqrt{-\frac{a}{2} + \frac{1}{2} \cdot \sqrt{a^2 + b^2}} \tag{4.19}$$

Substituting equation 4.14 into 4.19 yields equation 4.20.

$$u = \pm\sqrt{a + (-\frac{a}{2} + \frac{1}{2} \cdot \sqrt{a^2 + b^2})} = \pm\sqrt{\frac{a}{2} + \frac{1}{2} \cdot \sqrt{a^2 + b^2}} \tag{4.20}$$

Equation 4.20 will yield four solutions. However, from equation 4.13 it can be seen that the signs of u and v are equal if $b > 0$, and opposite if $b < 0$. Thus, for a case where $b \neq 0$, equation 4.20 can be written as shown in equation 4.21.

$$\sqrt{a + ib} = \pm\left(\sqrt{\frac{a}{2} + \frac{1}{2} \cdot \sqrt{a^2 + b^2}} + i\frac{b}{|b|} \cdot \sqrt{-\frac{a}{2} + \frac{1}{2} \cdot \sqrt{a^2 + b^2}}\right) \tag{4.21}$$

Thus, if we assume that $(k^2 - 4l)$ in equations 4.8 and 4.9 can be divided into a real part, a, and complex part, b, then the square root will be given by equation 4.21. This will in turn allow the eigenvalues λ_1 and λ_2 to be split into their real and complex parts.

That is, let $a = \mathrm{Re}(k^2 - 4l)$ and $b = \mathrm{Im}(k^2 - 4l)$, then equations 4.8 and 4.9 can be rewritten as is shown in equations 4.22 and 4.23.

$$\lambda_1 = \frac{k + \sqrt{a + ib}}{2} \tag{4.22}$$

$$\lambda_2 = \frac{k - \sqrt{a + ib}}{2} \tag{4.23}$$

By utilizing the relation in equation 4.21, this may further be rewritten as shown in equation 4.24 and 4.25.

$$\lambda_1 = \frac{1}{2} \cdot \left(k + \left(\sqrt{\frac{a}{2} + \frac{1}{2} \cdot \sqrt{a^2 + b^2}} + i\frac{b}{|b|} \cdot \sqrt{-\frac{a}{2} + \frac{1}{2} \cdot \sqrt{a^2 + b^2}}\right)\right) \tag{4.24}$$

$$\lambda_2 = \frac{1}{2} \cdot \left(k - \left(\sqrt{\frac{a}{2} + \frac{1}{2} \cdot \sqrt{a^2 + b^2}} + i\frac{b}{|b|} \cdot \sqrt{-\frac{a}{2} + \frac{1}{2} \cdot \sqrt{a^2 + b^2}}\right)\right) \tag{4.25}$$

The eigenvalues can thus be separated into their real and imaginary parts as shown below in equation 4.26 and 4.27,

$$\mathrm{Re}(\lambda) = \frac{1}{2} \cdot \left(p \pm \sqrt{\frac{a}{2} + \frac{1}{2} \cdot \sqrt{a^2 + b^2}} \right) \tag{4.26}$$

$$\mathrm{Im}(\lambda) = \frac{1}{2} \cdot \left(p \pm \frac{b}{|b|} \cdot \sqrt{-\frac{a}{2} + \frac{1}{2} \cdot \sqrt{a^2 + b^2}} \right) \tag{4.27}$$

where p denotes the real part of k, and q denotes the complex part of k.

Finally, the distance R from the point (-1,0) to any point on the curves λ_1 and λ_2 can be determined by equation 4.28 and 4.29 respectively.

$$R_1 = \sqrt{\left(\frac{p+2}{2} + \frac{1}{4}\sqrt{a + \sqrt{a^2 + b^2}} \right)^2 + \left(\frac{p}{2} + \frac{b}{4|b|}\sqrt{-a + \sqrt{a^2 + b^2}} \right)^2} \tag{4.28}$$

$$R_2 = \sqrt{\left(\frac{p+2}{2} - \frac{1}{4}\sqrt{a + \sqrt{a^2 + b^2}} \right)^2 + \left(\frac{p}{2} - \frac{b}{4|b|}\sqrt{-a + \sqrt{a^2 + b^2}} \right)^2} \tag{4.29}$$

The least distance $\mathcal{D}$, can then be found by analyzing the critical points of equation 4.28 and 4.29, as shown in equation 4.30 and 4.31.

$$\frac{dR_1(\omega)}{d\omega} = 0 \tag{4.30}$$

$$\frac{dR_2(\omega)}{d\omega} = 0 \tag{4.31}$$

It should also be noted that as the square root is a strictly growing function, the outer square root of equations 4.28 and 4.29 can be dropped in the minimization of R_1 and R_2 in equations 4.30 and 4.31.

In summary, if an analytical expression for the distance from the point (-1,0) to the curves of the eigenvalues, λ_1 and λ_2 can be established, then the least distance $\mathcal{D}$ from (-1,0) to one of the curves can be determined by evaluating equations 4.30 and 4.31. This expression of $\mathcal{D}$ could then be evaluated to yield exact values of the analytical model's stability assessment. This could probably be done quite efficiently in the converter's processor, as it would be a matter of plugging in parameters. The analytical model of the converter admittance would of course be known by the designer beforehand, and could be stored in the converter memory. The equivalent grid impedance would have to be determined on cite, but this could be converted into an analytical expression by the use of commonly known techniques of curve fitting.

Assuming that a suitable analytical expression for $\mathcal{D}$ could be established, the expression of $\mathcal{D}$ could be considered to be level surface in multidimensional space. The gradient vector of $\mathcal{D}$, $\nabla\mathcal{D}$, would then yield the change in each parameter that would give the greatest increase in $\mathcal{D}$. Thus, the gradient would directly yield which changes would increase the stability of the system. This information could in turn be used to issue adaptive control commands to change the controllable parameters in the converter.

Moreover, utilizing the directional derivative, the impact of any change in any parameter on the least distance $\mathcal{D}$, could be directly determined. For clarity, the directional derivative refers to the dot product between the gradient vector and a vector $\mathbf{u}$ containing the change in the selected parameter(s), $Du\mathcal{D}(x, y, ...) = \mathbf{u}\cdot\nabla\mathcal{D}(x, y, ...)$. This could be used to determine whether or not to allow certain changes, in for instance output current or voltage, when the system is close to the stability limit.

It could also be desired to not only keep the least distance $\mathcal{D}$ above some value, but also to do this with the minimum amount of change to the controller parameters. This is because the controller parameters are originally tuned for a specific purpose and should not be altered unnecessary. That is, the commanded change in the PLL and current controller gains should ideally be minimized to ensure minimal disturbance of the control system. The optimization could be done in many ways, but one simple alternative could perhaps be to use the well known method of Lagrange multipliers. In this case it would have to be augmented with Karush-Kuhn-Tucker conditions to accommodate inequality constraints [34]. It should, however, be noted that the Karush-Kuhn-Tucker conditions may for some cases not be sufficient for optimality. This would have to be determined via the analytical expressions.

Let the desired addition in distance $\mathcal{D}$, to make $\mathcal{D}$ greater or equal to some threshold, be denoted $\Delta\mathcal{D}$. Also let a change in a controllable parameter K_i be denoted ΔK_i. $L_{i,u}$ will denote greatest allowable increase in K_i, while $L_{i,d}$ denotes the greatest allowable decrease in K_i. Then the optimization problem becomes a sort of optimal dispatch problem, consisting of minimizing the expression in equation 4.32, subject to the constraints in equation 4.33 and equation 4.34.

$$\gamma = \sum_{n=1}^{N} |\Delta K_i| \tag{4.32}$$

$$\Delta\mathcal{D} - \sum_{n=1}^{N} \left(\frac{\partial\mathcal{D}}{\partial K_i} \cdot \Delta K_i \right) = 0 \tag{4.33}$$

$$L_{i,d} \leq K_i + \Delta K_i \leq L_{i,u} \ , \ i = 1, ..., N \tag{4.34}$$

In this case, N would be equal to 4, and the four parameters K_i would be the PLL and current controller proportional and integral gains. The allowable limits for

change of the gains, L_i, should be carefully determined for each case. It could also be an option to weigh the change in each parameter, to reflect which parameters could more readily be altered.

If the optimization could be carried out, the adaptive control would not only be able to determine the most effective actions to increase the system stability, it could also do this in the least intrusive way to the converter controller. However, there are some notes to be made. As it turns out, the analytical expressions grows very quickly in size through the derivation of the above expressions. Because of this, it was unfortunately not possible to explicitly create the above expressions in the permitted time and with the available computer resources. One possible solution to reduce the size of the expressions would be model reduction. However, as mentioned above, time did not permit for this to be implemented. Additionally, it could not be determined whether or not the Karush-Kuhn-Tucker method would be applicable without the explicit analytical expressions. Thus, this method is only included as a possible suggestion if the analytical expressions can be established in a further work.

4.3.1 Look-up-Table

Even though it was impossible to implement the procedure of the previous section analytically, it is still possible to implement the main idea numerically. This can be done by pre-calculating a set of recommended actions for a set of likely operating points, and storing them in a look-up-table. During operation, relevant parameters are inputted to the table, which then outputs the recommended actions. Some advantages of this is the simplicity of implementation, low computational requirements, and predictable controller outputs. One disadvantage is the limited number of operating points stored in the table. This necessitates interpolation of any values in-between such points, which in turn could give sub-optimal or even detrimental controller actions in some cases. Therefore, extra care should be taken when implementing such schemes, especially for non-linear systems.

The adaptive control by look-up-table could be implemented numerically in the following way: For each operating point to be tested, and for all relevant frequencies, all pieces of the model are evaluated and then combined into the equations 4.28 and 4.29. A search algorithm then finds the least distance $\mathcal{D}$. The acquisition can be sped up by letting the examined frequency range be in the vicinity of the previously found critical frequency. For each operating point that yields a minimal distance less than the threshold for activation, the partial derivatives of $\mathcal{D}$ is computed. This is done by finding the change in $\mathcal{D}$ for a change in one of the four controller gains. Several different step sizes should probably be applied to account for possible non-linearities in the system behaviour. From the list of possible candidates, i.e. different values of the control parameters, the best suited are selected and stored in the look-up-table. The term best suited refers to a choice of parameters that would give a sufficient distance $\mathcal{D}$ with minimal alteration of control parameters.

Chapter 5

Results, Analysis and Discussion

This chapter will present, analyze and discuss the main results of simulations, experiments, and analytical findings. First, a general explanation of how the simulations and experiments were implemented is presented. Second, the results of the impedance estimation are presented and analyzed. Third, some important analytical findings related to the converter model are explained, before the results of the stability analysis and adaptive control are presented. Note that a discussion of the results will be included in each section and will not be contained in a separate chapter.

5.1 Simulation- and Experimental-Setup

In order to try to assess the validity and performance of the previously presented models and methods, several simulations and some laboratory experiments were carried out. In both simulations and experiments, the system under test was made equal to that described earlier in this thesis, namely a 2L-VSC connected to a grid voltage trough a LCL-filter. To conduct the experiments, a separation transformer was included between the VSC and the emulated grid. This was subsequently included in the simulations and analytical stability assessment. The circuit parameters used can be found in table 5.1, while the default controller parameters used can be found in table 5.2.

Also note that in this chapter, values may be given in both absolute value and per unit. Details on the per unit system and applied base values can be found in appendix B.

Table 5.1: Circuit parameters

Element	Value
Converter side resistor	0.032 [Ω]
Converter side inductor	0.51 [mH]
Filter capacitor	49.7 [μF]
Grid side resistor	0.032 [Ω]
Grid side inductor	0.20 [mH]
Transformer resistance	0.128 [Ω]
Transformer inductance	0.82 [mH]

Table 5.2: Controller Parameters

Parameter	Value
Current control proportional gain	1.6
Current control integral gain	227,5
PLL proportional gain	0.511
PLL integral gain	28.35

5.1.1 Simulations and Software Tools

The numerical evaluation of equations was conducted in either Mathworks' Matlab software or Maplesoft's Maple software.

To validate and test the stability of the system, two different simulation models were used. Both were implemented in simulink software from Mathworks, utilizing the Simscape toolbox to model converters and circuit parameters.

The first model was a relatively simplified model. A 2L-VSC was modeled by an internal simulink average model. The control of this converter was implemented as described in section 2.3, and the converter was connected to an ideal voltage source via an LCL-filter. This simple model was used to avoid unnecessary complications in initial tests. For ease of reference, this model will be referred to as the simplified model throughout the rest of this chapter.

The second model, provided by SINTEF Energy, was a complete control system for an actual converter implemented in the simulink interface of the OP5600 platform from Opal RT. This model contained a current controller, VSC model, LCL-filter and an ideal voltage source in the same way as the first model. However, it also contained additional controllers, filters, and protection algorithms intended for laboratory implementation. This did not only give simulation results that would match reality more closely, but it also facilitated implementation of controllers in the laboratory equipment. This simulation model could also be uploaded to the OP5600 to run in real time simulations. Most of the simulation results presented later in this

thesis originate from the real time simulations on the OP5600 system. This model will be referred to as the real time model on the remainder of this chapter.

5.1.2 Experimental Setup

In addition to simulations, it was also desired to conduct experiments in the laboratory to test the validity of the proposed analytical models.

All of the experiments conducted for this thesis were carried out in the Smart Grid Laboratory at NTNU. To test the proposed stability assessment model, a 2L-VSC and LCL-filter were connected to a grid emulator through a separation transformer. The VSC is rated at 60KVA and based on Insulated Gate Bipolar Transistors (IGBTs). The implemented switching frequency was 10kHz. The grid emulator is a six output Egston CSU 200 Compiso System Unit rated at 200kVA. Three of the Egston terminals were used to emulate the three phases of the grid, while two other were used to maintain the dc-link voltage of the VSC. The control of the VSC was done by the mentioned SINTEF model through the simulink interface of the OP5600 platform.

5.2 Impedance Estimation

This section will present the implementation and results of the MLBS impedance estimation.

Several design criteria for the MLBS were presented in section 3.2.2. It was generally attempted to adhere to these criteria, but as it turned out several of them proved difficult to implement in practice. This is especially true for the generation frequency requirement of equation 3.4, which states that one of the generation frequency harmonics should lie at the fundamental frequency. One reason for this difficulty is that the memory blocks in simulink that were used to implement the shift register require the delay time to be a multiple of the simulation time step. This time step proved to be non-trivial to alter in the real time simulations, and was restricted to $100\mu s$. Because of severe time limitations, it was decided to accept non-ideal MLBS generation and neglect this criterion.

The MLBS can be included into the converter control in multiple ways. To avoid additional hardware or extra complications it was chosen to superimpose the MLBS signal on the current reference fed to the switches. This is perhaps the simplest and most common way to include the MLBS signal into the output current. The maximum length binary sequence itself was implemented via a shift register and XOR feedback described in appendix D.

5.2.1 Results of the Simplified Model

First, as an initial test, and to validate the post processing procedure, the MLBS was tested in the simplified simulink model. As mentioned previously, the simulation model was implemented in simulink by the utilization of an average switching model of a VSC, current controller with voltage feed forward and PLL as described in sections 2.3 and 2.3.1 respectively. The converter was interfaced to an ideal voltage source through an LCL-filter with parameters as given in table 5.1. All electrical model elements were collected from the Simscape toolbox of Simulink.

The MLBS was generated by a 5 bit shift register that produced a sequence of length 31. The length was chosen to ensure that it was larger than the settling time of the systems impulse response, as mentioned in section 3.2.2. The MLBS was furthermore injected approximately 140 times to reduce noise. In this model, without any real time constraints, a sampling time of $5\mu s$ was used.

The resulting impedance estimation is shown in figure 5.1, where the estimate is shown in black and the theoretical value is shown in blue color.

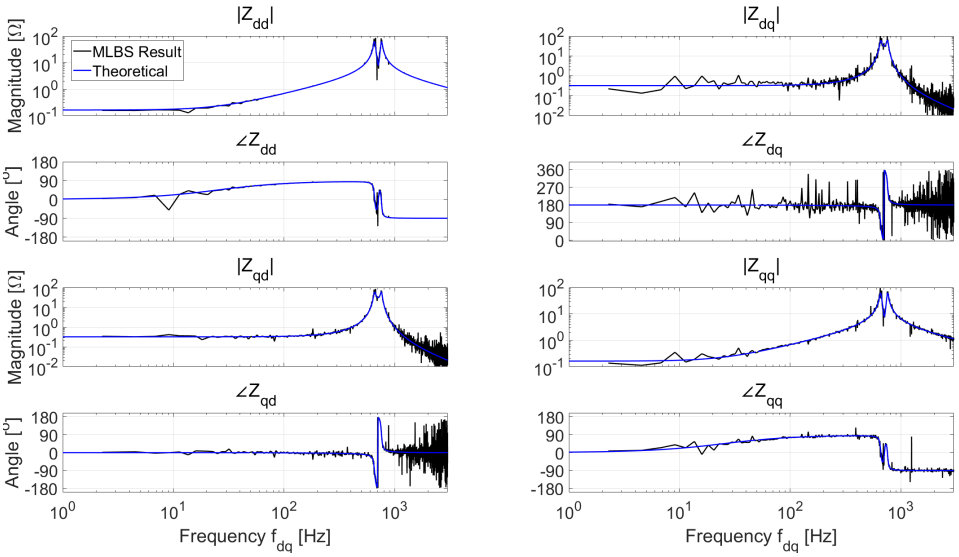

Figure 5.1: Impedance estimation of simplified system

From the above figure it can be observed that the estimates match very well with the theoretical value, although there are some deviations especially for high frequencies. This is expected as the injected sequence is not ideal and will thus cause some spectral leakage. The estimates will also be decreasingly accurate for higher frequencies as the signal energy drop. Additionally, the grid synchronization is not ideal, which will lead to further deviations in the estimates. These deviations may be alleviated in a simple manner by the use of post processing techniques such as a sliding average. Figure 5.2 depicts the same data set as that in figure 5.1, but

now the data has been subjected to a Gaussian-weighted moving average filter. The results exhibits a clear improvement and yields a near perfect result for a wide frequency range. One exception is the artificially created outliers for low frequencies. This can be corrected by better implementation of the moving average, but is neglected because of time restraints.

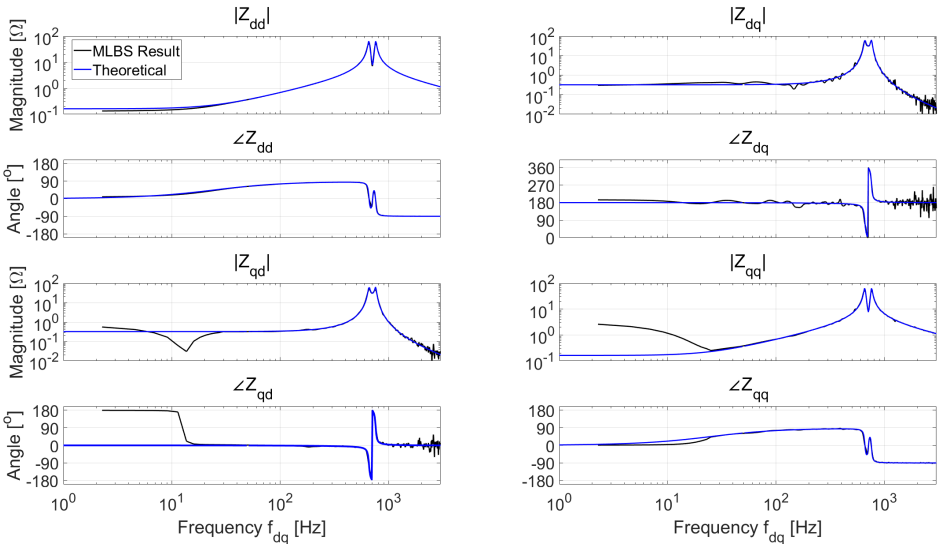

Figure 5.2: Averaged impedance estimation of simplified system

5.2.2 Real Time Model and Physical Experiments

The same experiment was repeated in the more complete real time simulation model, and as experiments in the lab. Both simulations and experimental implementation were then subject to real-time constraints. Figure 5.3 depicts the results of the simulations, while figure 5.4 depicts the experimental results. It is clear that neither simulations nor experiments yielded equivalent results as in previous section. As could be expected, both the simulation results and especially the experimental results contain additional noise. This is because they originate from less idealized systems that of figure 5.1. Also it is possible to observe the same trend in the shape of the impedances as that of the theoretical impedance. However, a highly unexpected observation is that the resonance peak of the impedance is shifted from approximately 600Hz in the ideal case, to approximately 2000Hz for both simulation and physical experiment. It should be observed that the results of the real time simulations and experiment match closely. Therefore, it can be assumed that the real time simulations and physical experiments indeed represent the same system. Furthermore, as an identical electrical grid was implemented in both the simplified and the real time simulations, it is natural to conclude that any errors in the estimate must originate outside erroneous model implementation.

One probable reason for the observed peak shift is the fact both the simulations and the laboratory experiment that were implemented in Opal RT, suffered from severe limitations on the achievable sampling rate. The limitations in sampling rate will increase the chance of aliasing effects and lower the captured frequency resolution etc. This suspicion originates from the fact that, in theory, basically the same MLBS was injected in all three tests. The main difference between the simplified simulations where the estimation succeeded, and the real time implementation, where the estimations failed, was the limited sampling rate. It should also be noted that the pure simulation will have perfect data capture, while the real time implementation will capture a number of points and then store the data in a file. If the saving of a file takes too long, the temporary memory can be overrun and data may be lost. If this happens the current and voltage waveforms are going to exhibit what appears to be an abrupt phase-shift. This will of course have a detrimental effect on the results of the FFT. Additionally, it was observed that when the MLBS was superimposed on the current reference, the outputted current was not able to follow this. It rather exhibited overshoots and seemingly erratic behaviour. This will probably be a contributing factor to the deviations in the estimates as the converter is not injecting a proper MLBS. Other possible contributors include: Added PLL dynamics that skew the measured currents and voltages, added aliases in the PWM scheme, or similar effects.

Because of these unexpected results, it was decided that the eigenvalues and stability assessment would be conducted exclusively by the use of theoretical values for the grid impedance. That is, for the remainder of this thesis, the grid impedance is assumed to be perfectly estimated for all relevant frequencies. However, identifying the effect that the real time implementation constraints has on a straightforward implementation of the MLBS is considered to be a contribution of this thesis, albeit overcoming such limitations are outside the thesis scope.

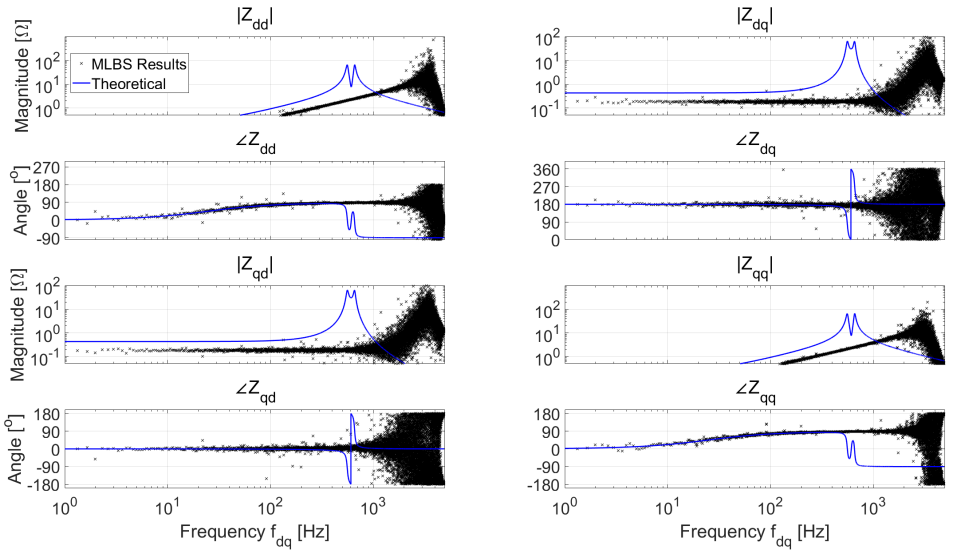

Figure 5.3: Impedance estimation in advanced simulation model

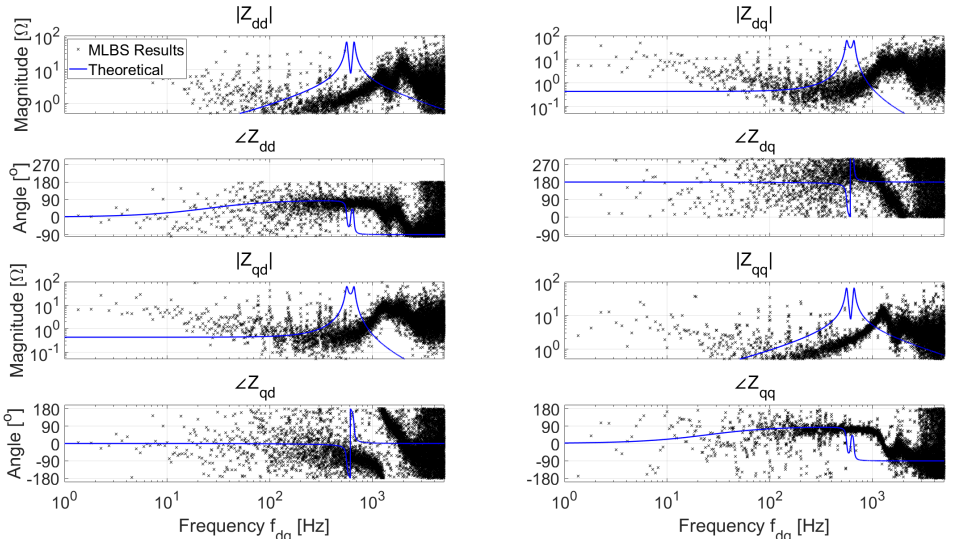

Figure 5.4: Experimental impedance estimation

5.3 Analysis of Analytical Expressions

In this section some key findings with regard to the analytical expressions are presented. First, a curious result of the inclusion of a voltage feed forward is explored, then some important numerical challenges are presented

5.3.1 Effect of Voltage Feed Forward

First note that the derivations of the equations used in this section can be found in appendix C. The mentioned equations will thus be presented and used directly without any further deliberations on their origin.

Consider the analytical equation of the converter dynamics, from switch terminal voltage, denoted v_t, to converter output terminal voltage, denoted v_s. This is the same expression as in equation C.12, repeated below for reference.

$$\begin{bmatrix} sL+R & -L\omega_0 \\ L\omega_0 & sL+R \end{bmatrix} \cdot \begin{bmatrix} i_d^s \\ i_q^s \end{bmatrix} = \begin{bmatrix} v_{td}^s \\ v_{tq}^s \end{bmatrix} - \begin{bmatrix} v_{sd}^s \\ v_{sq}^s \end{bmatrix} \tag{5.1}$$

The switch terminal voltage, v_t, is the control input. If the controller contains both decoupling terms and a voltage feed forward action, and PLL and delay effects are assumed negligible, then v_t may be expressed as shown in equation 5.2.

$$\begin{bmatrix} v_{td}^s \\ v_{tq}^s \end{bmatrix} = \begin{bmatrix} H_{PI} & 0 \\ 0 & H_{PI} \end{bmatrix} \cdot \begin{bmatrix} i_d^* - i_d^s \\ i_q^* - i_q^s \end{bmatrix} + \begin{bmatrix} 0 & -L\omega_0 \\ L\omega_0 & 0 \end{bmatrix} \cdot \begin{bmatrix} i_d^s \\ i_q^s \end{bmatrix} + \begin{bmatrix} v_{sd}^s \\ v_{sq}^s \end{bmatrix} \tag{5.2}$$

where the superscript * denotes the current reference value.

If equation 5.2 is substituted into equation 5.1, it is obvious that the converter terminal voltage is canceled by the perfect "estimate" of the feed forward. The converter may in this case be interpreted to only be a current source whose output is independent of the grid impedance. Assuming the grid to be stable by itself, the converter will be stable for any value of the grid impedance, according to this model.

In a less idealized case, the converter output terminal voltage will be reintroduced through the PLL effects and possible feed forward measurement delays. This can be seen by referring to section 2.3.1 or appendix C. However, as the matrices in the PLL equations 2.25, 2.27, and 2.29 does not include the d-axis voltage, only the q-axis voltage will be reintroduced through the PLL effect. The inclusion of a delay in the voltage feed forward will hinder the perfect cancellation of the converter output voltage. However, this makes the stability assessment sensitive to a parameter which is both difficult to determine and is not constant in practical implementations. Furthermore, both the PLL effect and feed forward delay will evaluate to small numerical values that will be prone to rounding errors unless care

is taken. This will be increasingly true as the measurement delays are reduced and the PLL performance is increased. Because of this, the accuracy of the model may be challenged by numerical constraints.

Based on the above discussion it is clear that the voltage feed forward delay should not be neglected, when modeling the system for impedance representation. It should furthermore be carefully determined to avoid loss of accuracy. Because of this, the commonly used estimates of the delay as presented in section 2.3.2 may be used as a starting point, but should most likely be refined for the actual system to be implemented. In a practical implementation it should also be ensured that all computations are done to ensure sufficiently accurate estimates. The latter will be the topic of the next section.

5.3.2 Numerical Challenges

As it turned out, the work with this thesis was plagued by numerical difficulties. Upon completion of the model equations, these were implemented in Matlab code and evaluated. The numerical evaluation of this provided a lot of false results that were largely inconsistent with simulations, which caused a great deal of confusion. As a reaction to this, a great effort and huge amount of time was spent on trying to validate the analytical model. The equations were checked and re-derived from first principle relations. All simulation files were also checked and double-checked for errors.

When no solution to the erroneous results could be found, it was decided to attempt to implement the expressions in another software in case there were some unfortunate effects in internal functions of Matlab. The equations and relations where implemented symbolically, step by step, in Maple. This yielded greatly improved results. The symbolical implementation also yielded another important result. If all parameter values were substituted into the vast equations, it was found that the expressions for the eigenvalues contained terms of angular frequency, ω, to the power of 78. It was also found that some of the coefficients were in the order of magnitude of ten to the power of 108. Such expressions will of course not be numerically stable, and could explain the inconsistent results. One reason for this vast power originated from the choice of approximating the delays by the second order Padé equation in section 2.3.2. By using the 1.st order Padé the angular frequency was reduced to the power of 20. This is a great improvement although the equations will still be numerically 'ticklish'. Depending on how the equations are implemented and solved in the software solution, it may also be possible to utilize the exponential of equations 2.31 and 2.32 directly to further reduce this problem. As available time did not permit further attempts to refine the analytical expressions, through for instance model reduction, it was decided that the stability assessment and adaptive control would be implemented purely numerically. That is, the equations were evaluated numerically for each step, and each building block, and finally combined to the final eigenvalues for each frequency. This was done to

avoid the detrimental propagation of terms that grow to unmanageable sizes. This last solution did finally yield accurate and consistent results.

From the above discussion it can be concluded that great care should be taken in the numerical evaluation of the presented equations and relations. If not, the stability assessment is prone to false results, at least for the case chosen herein. The original decision to implement the complete relations instead of a step by step numerical implementation originated from the desire to avoid propagating rounding errors. This did, however, prove to be counterproductive, and should be attributed to lack of experience. It should also be noted that the large effort made to solve the mentioned problems, unfortunately severely limited the available time for producing other results.

5.4 Stability Assessment and Adaptive Control

This section will present the results of the stability assessment method and the effect of a simple adaptive control scheme.

5.4.1 Stability Assessment

The stability assessment procedure was tested by comparing the point where the real time simulation model tipped into instability with the point that was predicted by the analytical model.

As the stability assessment model was implemented numerically, it was not possible to solve the model and find the exact point at which one of the eigenvalues encircled the (-1,0) point. The assessment was rather implemented graphically. That is, plots were created for each case and assessed for instability. An algorithm that iterated through the relevant frequencies to determine the minimum distance from the curves to the point (-1,0) was created to aid this assessment. An added uncertainty in this determination is nonetheless expected as it is not feasible to check every possible frequency. An example of such a plot is shown in figure 5.5. Figure 5.6 depicts the same plot only zoomed in on (-1,0) point. It will be difficult to find close to exact results using a discrete approach, as this would require the testing of a very large number of values. Some deviations is therefore expected in the estimates, not only because of discrete steps in the frequencies examined but also because of the discrete steps in for instance the grid impedance.

For simplicity, only the inductive part of the grid impedance was increased in the tests. This was done in steps of 0.2mH. Thus, all results presented below have a uncertainty of at least $\pm$0.2mH. Consider figure 5.7 which depicts the case where the converter exceeds the tipping point of instability.

Figure 5.7c depicts the case where the grid inductance is increased from approximately 9.8mH to approximately 9.98mH. At this point resonance between the

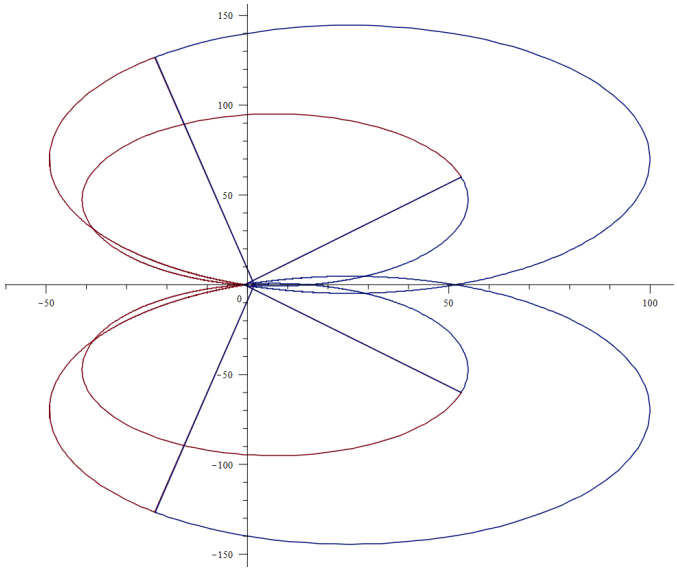

Figure 5.5: Example plot of eigenvalue curve created by the analytical model close to instability

converter and grid is induced. Oscillations can be observed in the PLL output immediately afterwards, shown in figure 5.7b. The output of the PLL shown here is the estimated grid frequency in Hertz. The actual grid frequency was kept at a perfect 50Hz, thus all oscillations are due to controller malfunction. Equivalent oscillations are also induced in the current controller output. Figure 5.7a depicts the immediate and oscillatory response in the converter output current. The oscillations in the PLL output frequency, and current controller output signals, propagate through the control system and cause a growing oscillation in the peak amplitude of roughly 4Hz. These oscillations grow quickly, and unacceptable operating conditions are reached in seconds.

The above simulations showed that the limit of stability was located somewhere between approximately 9.8mH and 9.98mH added grid inductance. The stability assessment from the analytical model predicted this limit to be located somewhere between 11.4 and 11.6mH. The deviation between the two are thus less or equal to 16.2%. There are several possible reasons for this deviation. These include, the inaccuracies mentioned at the start of this section and rounding errors in both simulation- and analytical model. Other possible contributors are the extra effects included in the converter control of the advanced model but not in the analytical model. The two models showed less or equal deviations for other configurations and circuit parameters. It can also be argued that to consistently be accurate within 16.2% is acceptable for such a simplified model.

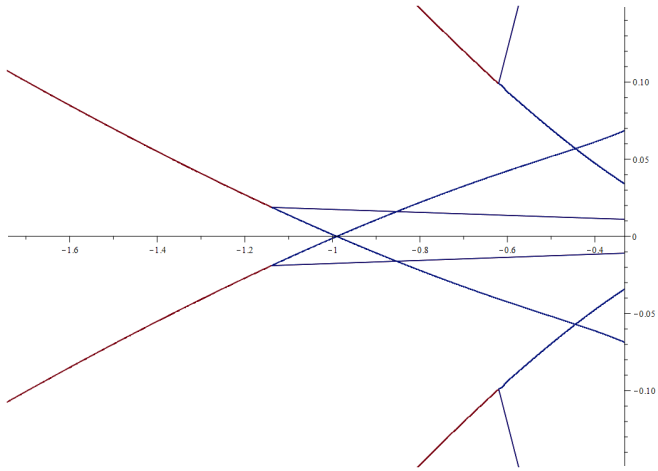

Figure 5.6: Example plot of eigenvalue curve created by the analytical model close to instability, zoomed in on (-1,0)

5.4.2 Adaptive Control

A simple adaptive control scheme was tested in the same case as was used in the previous section. That is, when the grid inductance is increased from approximately 9.8mH to 9.98mH and oscillations are induced. A zoomed out overview of the controller and output current behaviour is depicted in figure 5.8. Note that here, also the current controller output is included in figure 5.8c. The current control output exhibits equivalent behaviour to that of the PLL output. As can be seen in the figure, after the step increase in the grid inductance at approximately 243.25s, oscillations are immediately induced in the controller outputs. The oscillations grows exponentially until striations that limits further growth are reached. These saturation effects are not included in the analytical model but are included in the advanced converter controller as a safety measure. Without these saturation effects, the output in a physical system would grow without bounds until the system protection switches tripped or some component was destroyed. At approximately 253.75s, the adaptive controller is activated and issues appropriate scaling signals to the four controllable parameters. These are, the proportional and integral gains of the PLL and current controller PI. The system subsequently returns to stable operation within approximately 1.5 to 2 seconds.

The adaptive control was implemented numerically as a simple look up table, as proposed in section 4.3.1. The look up table was calibrated to account for some of the deviation discovered in the previous section. Some margins were still kept in the calibration. Due to time limitations the table was quite rough with steps of 5%. The gains were also scaled together. That is, the integral and proportional gains of the current control PI was scaled as one, and not individually. The same applies for the PLL PI gains. A simple attempt of optimizing the scaling to minimize

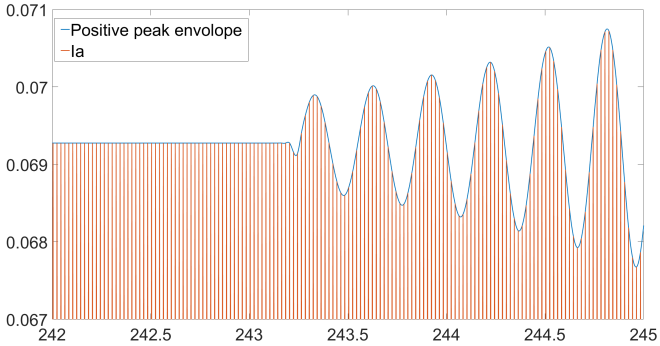

(a) Line Current [p.u.] and Envelope

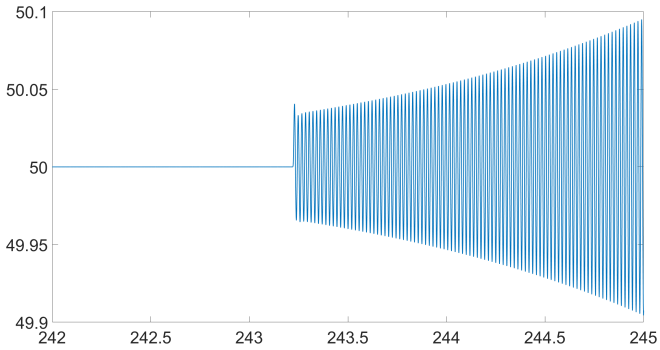

(b) PLL Controller Output [Hz]

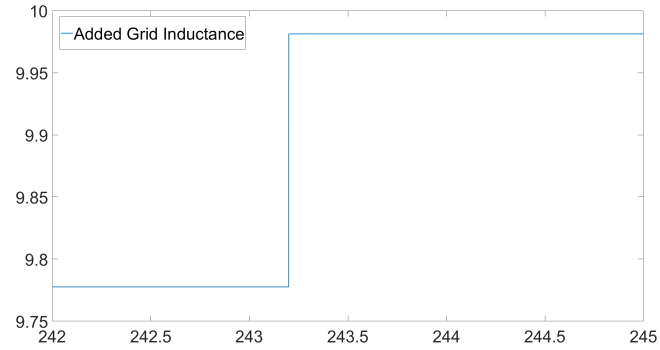

(c) Grid Inductance [mH]

Figure 5.7: Simulation results of the converter exceeding the tipping point of stability

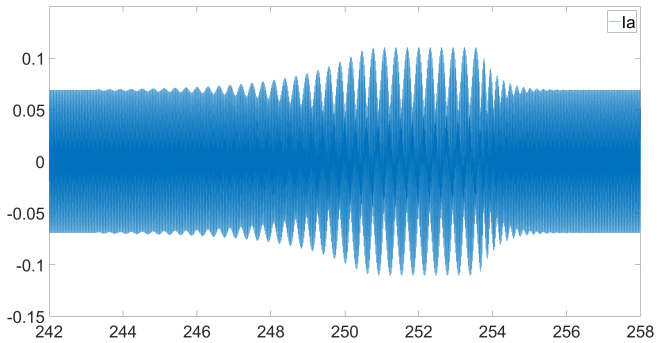

(a) Line Current [p.u.]

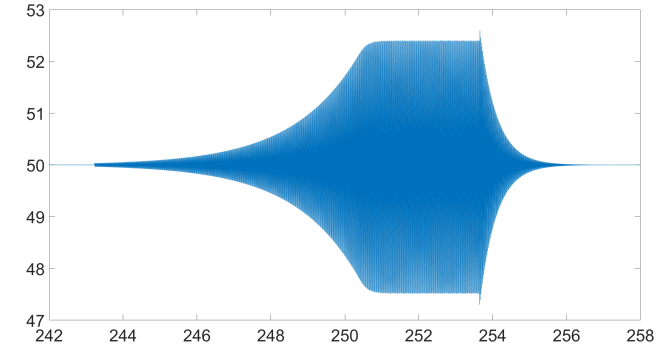

(b) PLL Controller Output [Hz]

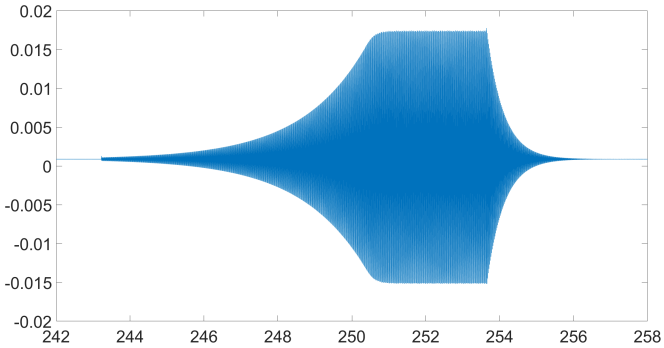

(c) Current Controller Output [p.u.]

Figure 5.8: Overview of simulation results portraying instability event

the changes in parameters was pre-calculated and included in the table. A close up of the adaptive controller action, and its effect, is shown in figure 5.9. At

approximately 253.75s, the adaptive control is activated, and issues scaling signals to the controller gains. The issued scaling is shown in figure 5.9c. The term K.PLL.i.sc shows how the PLL controller's integral gain is scaled, K.c.p.sc shows how the current controller's proportional gain is scaled, and so on. As can be seen in the figure, the adaptive control issues commands to increase both PLL and current controller gains by approximately 1.088. This is calculated to be sufficient to bring the system back to stable operation. The response in the PLL output and converter output current can be seen in figures 5.9b and 5.9a respectively. The oscillations decay to acceptable values withing 1.5 to 2 seconds and disappears completely in a few additional seconds. From this it is clear that the adaptive controller works as intended and returns the system to stable operation after instability was triggered. The simple optimization also works as it takes what would have been a scaling of 10% down by 1.2% to 8.8%, although considerable margins are still being taken.

Lastly it should be noted that despite best efforts it was not possible to implement and test the stability assessment in an experimental setup. This should be included in a further work to properly validate the proposed method against real life systems and not only simulations.

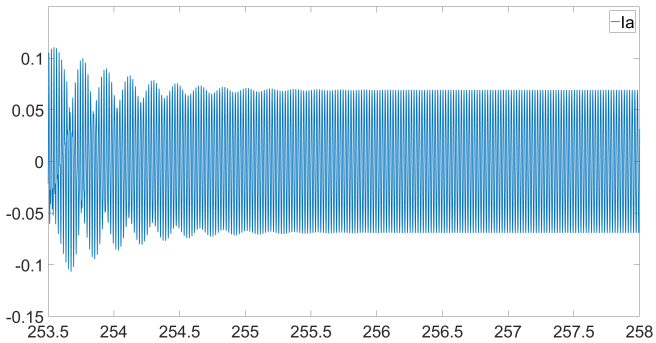

(a) Line Current [p.u.]

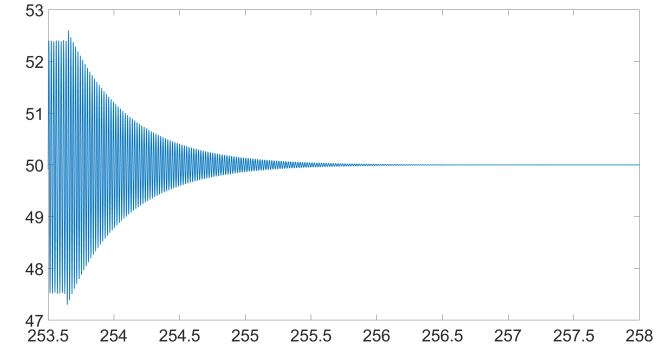

(b) PLL Controller Output [Hz]

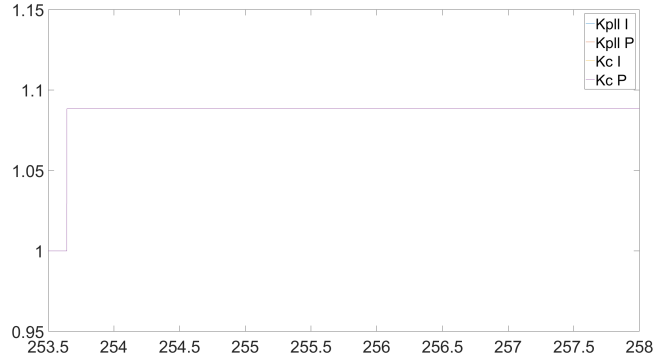

(c) Adaptive Control Scaling Signal

Figure 5.9: Simulation results of an adaptive controller action to recover from instability

Chapter 6

Conclusion and Further Work

6.1 Conclusion

Through the work in this thesis, the theoretical foundation of the grid impedance method was laid out. A suitable analytical model of a 2L-VSC and control scheme was then created. Based on the above, a stability criterion for the converter was deduced and implemented. In a realistic implementation of the proposed method, the grid impedance would be unknown and would need to be estimated. Several possible methods to do so were briefly reviewed. The MLBS was selected for use in this thesis in accordance with the guidelines outlined in the introduction. Subsequently, the key theoretical features of the MLBS were explained, and the impedance estimation method was implemented. The implementation consisted of simulations in both a simplified and a more advanced model containing real time constraints, as well as laboratory experiments. Lastly, an adaptive control to increase the stability of the converter was proposed, deduced and implemented.

Based on the results and discussion presented in chapter 5, it is possible to conclude that the stability assessment procedure deduced in this thesis performed well under testing. The deviation between analytical model and real time simulations was found to be less or equal than 16%. Such a deviation could be expected, and furthermore considered to be minor, when taking into account the fact that not all elements contained in the real time simulations were present in the analytical model. This fact can additionally be interpreted as an indication that the proposed model and associated stability assessment, could be applied to more complex systems with acceptable accuracy. The latter must however be further explored before any clear conclusions can be drawn. The work with the stability assessment method also encountered severe numerical difficulties in the evaluation of the analytical model.

This discovery, and the highlighting of which, may be considered an important result of the work in this thesis. This is because, it does not only exhibit the numerical difficulties that may be encountered in such implementations, or highlight a possible need for model reduction, but also because it can serve as a foundation for other efforts to implement similar schemes. As such, it may be concluded that the former is an additional small contribution of this thesis.

The results of the grid impedance estimation method showed very good results in the simplified simulation model. It may thus be concluded that sequence design and post processing were implemented successfully. The good results also indicate that the MLBS is suited for the use intended in this thesis. The implementation in real time execution did however, not exhibit the same compliance with the theoretical values, neither for the simulations nor for the laboratory experiment. As the real time simulation and laboratory experiment matched closely with each other, it can be concluded that the tests represented the same system. In turn, it could be concluded that the deviations in the estimates originated from the constraints posed by the real time implementation, and not erroneous construction of the simulation or experiment. This can moreover be considered one of the main contributions of this thesis, namely to display the effect that real time constraints have on the straightforward implementation of the MLBS methodology from pure simulation to real time implementation. It may also be concluded that the real time constraints on the sampling time and data-integrity should be carefully considered in future implementations.

The proposed adaptive controller was first developed analytically. It could however, not be implemented by analytical expressions as they became too large even for computer aided tools. If such an implementation had succeeded, it would probably in any case have encountered the same numerical difficulties as that of the stability assessment described in section 5.3.2. The proposal of the analytical expressions for the adaptive control, may nonetheless be considered to be a valuable theoretical contribution of this thesis. This is because it may serve as a foundation or inspiration to other efforts. Furthermore, if model reduction or similar techniques can be utilized to successfully reduce the analytical expressions to a manageable size, the proposed adaptive controller could be implemented directly. The proposed adaptive control was also implemented numerically. That is, all analytical expressions were evaluated numerically before they were pieced together to form the full model expressions. For the test case shown in section 5.4.2, it may be concluded that the adaptive control succeeded in its primary and secondary objectives. That is, to increase the stability of the system and to do so while minimizing the alteration of controller parameters. The results may thus be seen as an indication that the proposal for adaptive controller is sound.

6.2 Further Work

Several inclusions could be made in a further work and a continuation of the efforts of this thesis. These would hopefully aid on the way towards the final goal of creating a methodology that could be commonly applied in generic PECs to allow stable plug-and-play capabilities.

Such efforts could include:

1. Explore if the relatively simple analytical model, which omits outer control loops in its current form, is applicable to systems containing more complex control systems, with sufficient accuracy.
2. Expand the modeling to include possible unbalances in the three phase system, and examine the effect of these. Such imbalances are especially present during certain faults. These could be relevant to the fault-ride-through capabilities of the converter. The effect of imbalances could perhaps be included in the adaptive control that, upon detection, would ensure stability in the fault-ride-through period.
3. Implement model reduction or other such techniques to allow for the creation and further analysis of the full analytical expressions developed. This could facilitate the implementaion of the theoretical discoveries.
4. Include quasi-passive behaviour in the grid impedance estimation. It would also be desirable to develop some sort of sensing and adaptive control to avoid several converters injecting MLBS' simultaneously.
5. Optimize on-line stability assessment, grid impedance estimation, and adaptive control action with regard to time. If this optimization can be carried out successfully, it would facilitate online implementation in actual systems.

Appendices

Appendix A

DQ-frame

A more thorough explanation of the dq-system can be found in [16], while some of the most important features of the dq system for this thesis will be presented in this section.

A conventional three phase system will contain three sinusoidal components displaced 120° from each other in time. However, a conventional linear PI controller will generally not be able to regulate a sinusoidal input with no steady state error [16]. Therefore, the design of the control of such a system would be more complicated than for conventional linear control. One way to avoid some of this complication is to introduce the dq-system. This is mainly a mathematical transformation, but one graphical interpretation is described below.

A three phase set of currents and/or voltages can be represented in space vector form along three axes, a, b, and c, distributed 120° from each other in space. These three components can be added together into a single voltage or current phasor that rotates with the angular velocity ω_g. $\omega_g = 2\pi f_g$, and f_g is the electrical frequency of the system. Let d and q denote two orthogonal axes that are free to rotate about the origin. Note that different conventions exist in different references, but in this thesis the q-axis is chosen to lead the d-axis. Referring to figure A.1, the dq-frame with angular velocity ω_c is depicted together with the system voltage phasor v_g with angular velocity ω_g. Also the stationary phase a axis is included for completeness.

Consider the case where $\omega_g = \omega_c$, i.e. the dq-axes and voltage phasor are rotating at the same angular velocity. Then the phasor, or equivalently the abc- sinusoidal phase components, could be projected onto the d- and q-axis resulting in constant quantities. Thus, sinusoidal AC signals in the stationary abc-reference frame can be transformed into DC components in the rotating dq-reference frame. This would in turn allow for the use of simple conventional linear control techniques.

As mentioned in section 2.2, this mapping from abc- to dq-frame can be done math-

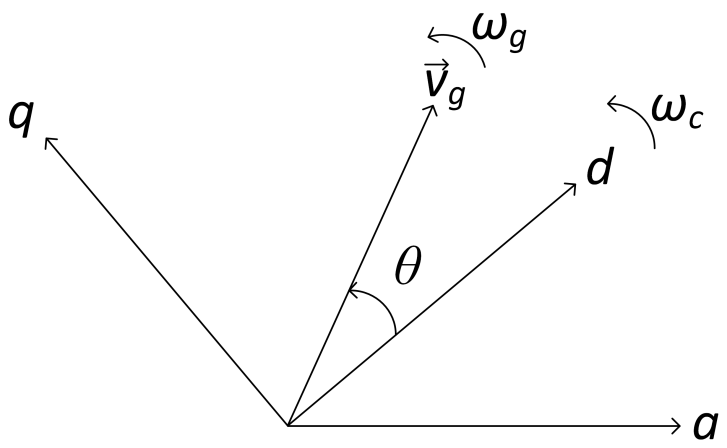

Figure A.1: Relation between a-axis, grid voltage phasor and the dq-axes

ematically by the help of the Park transformation. There are several alternative forms that could be used, but the one shown in equation A.1 [16] is adopted in this thesis.

$$\begin{bmatrix} V_d \\ V_q \end{bmatrix} = \frac{2}{3} \cdot \begin{bmatrix} \sin(\theta) & \sin(\theta - \frac{2\pi}{3}) & \sin(\theta + \frac{2\pi}{3}) \\ \cos(\theta) & \cos(\theta - \frac{2\pi}{3}) & \cos(\theta + \frac{2\pi}{3}) \end{bmatrix} \cdot \begin{bmatrix} V_a \\ V_b \\ V_c \end{bmatrix} \tag{A.1}$$

The angle Θ in equation A.1 is the same as that in figure A.1.

It should be noted that the above graphical interpretation and mathematical transformation applies for a balanced three phase system. Generally, the Parks transform also contain a 0-component, forming a dq0 system that takes any imbalances into account. Since the tree phases are assumed to be balanced in this thesis, the 0-components would only contain zeros, and is therefore omitted.

A last consideration to be made in regards to the dq reference frame modeling, is that the transformation contains one degree of freedom. The angle Θ may be chosen freely at convenience. One common choice, which is also adopted in this thesis, is to choose Θ to be zero, i.e. to align the d-axis with the system voltage phasor. The q-axis system voltage is then equal zero in steady state. This will simplify the power control from MIMO to SISO and is an important reason for this choice. The active and reactive power in dq-reference frame is given by equation A.2 and A.3 respectively [16].

$$P(t) = \frac{3}{2} \cdot (v_d(t) \cdot i_d(t) + v_q(t) \cdot i_q(t)) \tag{A.2}$$

$$Q(t) = \frac{3}{2} \cdot (-v_d(t) \cdot i_q(t) + v_q(t) \cdot i_d(t)) \tag{A.3}$$

By inspection it is clear that by letting the q-axis voltage component be equal to zero, the active and reactive power of the converter could be regulated independently by the d- and q-axis currents respectively. The latter power control is not implemented in this thesis, but the above consideration is still included for reference, as it would be included in a more complete controller model and could be considered in further work.

Appendix B

Per-Unit values

The point of transforming equations into Per Unit (p.u.), is to scale the equations into a simpler form where most values lie in the range of 0 to 1. Similar systems of different ratings can furthermore be compared directly based on the p.u. system. The requirement to this scaling is coherence through all the relations that normally apply to the system. These, and the numeric base values are shown in section B.1. A p.u. value is simply a scaled value as shown below.

$$X_{p.u.} = \frac{X_{actual}}{X_{base}} \tag{B.1}$$

B.1 Base Values

The base values herein are chosen in accordance with the experimental setup in the Smart Grid laboratory at NTNU. The base voltage is chosen to be the the specified line-to-line (ll), root mean square (RMS) voltage of the voltage supply. The base power is similarly chosen to fit the power rating for the converter under test. All other base values are then deduced from the initial two, in accordance with the applicable circuit relations. This is shown in equation B.2 to B.8 below.

$$V_{base,line-to-line,RMS} = 400[V] \tag{B.2}$$

$$S_{base} = 50[kVA] \tag{B.3}$$

$$v_{base,phase-to-neutral,peak} = \sqrt{\frac{2}{3}}\, V_{base,line-to-line,RMS} \tag{B.4}$$

$$i_{base,line,peak} = \sqrt{\frac{2}{3}} \frac{S_{base}}{V_{base,line-to-line,RMS}} \tag{B.5}$$

$$Z_{base} = \frac{i_{base,line,peak}}{v_{base,phase-to-neutral,peak}} \tag{B.6}$$

$$L_{base} = \frac{Z_{base}}{\omega_{base}} \tag{B.7}$$

$$C_{base} = \frac{1}{Z_{base} \cdot \omega_{base}} \tag{B.8}$$

The resulting values are summarized in table B.1 below.

Table B.1: *Adopted base values of the p.u. system*

Quantity	Symbol	Value
Power	S_b	200 kVA
Voltage	$V_{b,ll,RMS}$	400 V
Voltage	$v_{b,ph,peak}$	326,6 V
Current	$i_{b,peak}$	102,06 A
Frequency	ω_b	100π rad/s
Impedance	Z_b	3,2 Ω
Inductance	L_b	10,19 mH
Capacitance	C_b	994.7 μF

B.2 Perunitization of Equations

This section will show how to transform equation 2.13 and 2.14 into the per unit (p.u.) system. The other equations in connection with the converter modeling are those related to the control system, and as such does not need to be scaled to p.u. in the same way as the physical system. Furthermore, as the procedure will be identical, only equation 2.13 is transformed explicitly.

Equation 2.13 is repeated below for reference without the tilde notation.

$$L\frac{d}{dt}i_{td} = L\omega_0 \cdot i_{tq} - R \cdot i_{td} + \frac{V_{DC}}{2} \cdot m_d - v_{sd} \tag{B.9}$$

If both sides of the equation are multiplied with L, all terms in equation B.9 are voltages. Therefore, both sides can be scaled by the base value v_b of section B.1.

$$\frac{L\frac{d}{dt}i_{td}}{v_b} = \frac{L\omega_0 \cdot i_{tq}}{v_b} - \frac{R \cdot i_{td}}{v_b} + \frac{\frac{V_{DC}}{2} \cdot m_d}{v_b} - \frac{v_{sd}}{v_b} \tag{B.10}$$

From equation B.6 it is clear that $v_b = Z_b \cdot i_b$, and equation B.7 states that $Z_b = \omega_b \cdot L_b$. Substituting this into equation B.10 yields

$$\frac{L\frac{d}{dt}i_{td}}{\omega_b \cdot L_b \cdot i_b} = \frac{L\omega_0 \cdot i_{tq}}{\omega_b \cdot L_b \cdot i_b} - \frac{R \cdot i_{td}}{Z_b \cdot i_b} + \frac{V_{DC,p.u}}{2} \cdot m_d - v_{sd,p.u} \tag{B.11}$$

or

$$\frac{L_{p.u}}{\omega_b}\frac{d}{dt}i_{td,p.u} = L_{p.u} \cdot \omega_{0,p.u} \cdot i_{tq,p.u} - R_{p.u} \cdot i_{td,p.u} + \frac{V_{DC,p.u}}{2} \cdot m_d - v_{sd,p.u} \tag{B.12}$$

It should be noted that the term ω_b is a mathematical convenience only, and does not indicate that time itself is scaled, which its not. That is, any use of ω to denote time through frequency will not be scaled by ω_b. The term ω_b is exclusively used for convenience in relation to scaling the impedance of an inductor or a capacitor.

Appendix C

Analytical Converter Model Equations

This section will expand on the equations of the analytical converter model skipped earlier for compactness.

In section 2.3, the matrix block diagram of the complete small signal linear 2L-VSC model was presented in figure 2.11. This is repeated below for reference.

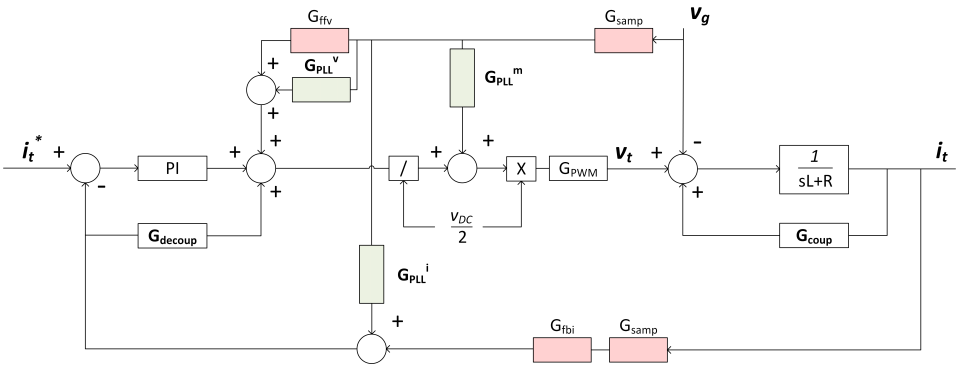

Figure C.1: Complete converter model including current control, decoupling, effects of measurements, sampling, PWM, and PLL effects included

The blocks $\mathbf{G_{coup}}$ and $\mathbf{G_{decoup}}$ are given in equation C.1 and C.2 below.

$$\mathbf{G_{coup}} = \begin{bmatrix} 0 & L\omega_0 \\ -L\omega_0 & 0 \end{bmatrix} \tag{C.1}$$

$$\mathbf{G_{decoup}} = \begin{bmatrix} 0 & -L\omega_0 \\ L\omega_0 & 0 \end{bmatrix} \tag{C.2}$$

The PI block symbolizes the well known PI controller, whose transfer function generally will be given as in equation C.3 below,

$$H_{PI}(s) = K_p + \frac{K_i}{s} \tag{C.3}$$

where K_p is the proportional gain and K_i is the integral gain.

If the PI controllers on the d and q axis currents have the same parameters, equation C.3 can be used directly. This is the case in this thesis. Otherwise, it must be converted into matrix form to capture the different parameters on the d and q axis.

The derivation of the matrices $\mathbf{G}^m_{PLL}$, $\mathbf{G}^i_{PLL}$, and $\mathbf{G}^v_{PLL}$ are given explicitly in section 2.3.1 while the effect of the PWM and sampling of the G_{PWM} and G_{samp} blocks are given explicitly in section 2.3.2. The G_{ffv} block indicates the voltage feed forward filter used to reduce noise in the measurements. Likewise, G_{fbi} indicates the filter on the feed back measurements of the current. If a first order filter is used for both G_{ffv} and G_{fbi}, they will be represented as shown in equation C.4

$$G_{filter}(s) = \frac{1}{1 + s/\omega_c} \tag{C.4}$$

where ω_c is the filter cutoff frequency. Note that care should be taken when designing these filters, as they inevitably will influence the dynamics of the system.

In section 2.4, the stability of the system was shown to depend on the equivalent output admittance of the converter, $\mathbf{Y_o}$. That is, the matrix equation from converter terminal voltage $\mathbf{v_t}$ to converter output current $\mathbf{i_t}$ as shown in equation C.5 below.

$$\begin{bmatrix} i_{td} \\ i_{tq} \end{bmatrix} = - \begin{bmatrix} Y_{dd} & Y_{dq} \\ Y_{qd} & Y_{qq} \end{bmatrix} \cdot \begin{bmatrix} v_{t,d} \\ v_{t,q} \end{bmatrix} \tag{C.5}$$

Again, note that the minus sign appears because the reference current direction is defined to be out of the converter.

The equivalent output admittance can be deduced by utilizing the principle of superposition on the linear system in figure C.1. The equations are too large to fit the page in expanded form, and will therefore be given in compact form below by the use of some compacting variables.

For clarity, the following relations are used in addition to what has been stated already, while the variables are stated in table C.1.

$$H_{pll} = \frac{K_{pll,i}}{s} + K_{pll,p} \tag{C.6}$$

$$G_{v,samp} = G_{i,samp} = \frac{(0.5T_s \cdot s)^2 - 6 \cdot 0.5T_s \cdot s + 12}{(0.5T_s \cdot s)^2 + 6 \cdot 0.5T_s \cdot s + 12} \tag{C.7}$$

$$G_{PWM} = \frac{(1.5T_s \cdot s)^2 - 6 \cdot 1.5T_s \cdot s + 12}{(1.5T_s \cdot s)^2 + 6 \cdot 1.5T_s \cdot s + 12} \tag{C.8}$$

$$G_{vff}(s) = \frac{1}{1 + s/\omega_{vff}} \tag{C.9}$$

$$G_{fbi}(s) = \frac{1}{1 + s/\omega_{fbi}} \tag{C.10}$$

$$\mathbf{I} = \begin{bmatrix} 1 & 0 \\ 0 & 1 \end{bmatrix} \tag{C.11}$$

First, consider the physical part of the converter system. That is, from the switch terminals, past the first filter inductor,and out to the converter system boundary. The equations modeling this system can be written as shown in the matrix equation C.12, in Laplace domain.

$$\begin{bmatrix} sL + R & -L\omega_0 \\ L\omega_0 & sL + R \end{bmatrix} \cdot \begin{bmatrix} i^s_{td} \\ i^s_{tq} \end{bmatrix} = \begin{bmatrix} v^s_{td} \\ v^s_{tq} \end{bmatrix} - \begin{bmatrix} v^s_{sd} \\ v^s_{sq} \end{bmatrix} \tag{C.12}$$

v_t denotes the switch terminal voltage, v_s denotes the system/converter interface voltage, and i_t denotes the converter current. Superscripts s and c denotes physical system reference frame and controller reference frame respectively, in the same way as in section 2.3.1.

The switch terminal voltage is the quantity that is being controlled, and this can be written as shown in equation C.13.

$$\begin{bmatrix} v^c_{td} \\ v^c_{tq} \end{bmatrix} = \begin{bmatrix} H_{PI} & 0 \\ 0 & H_{PI} \end{bmatrix} \cdot \begin{bmatrix} i^*_{td} - D \cdot i^c_{td} \\ i^*_{tq} - D \cdot i^c_{tq} \end{bmatrix} + \begin{bmatrix} 0 & -L\omega_0 \\ L\omega_0 & 0 \end{bmatrix} \cdot \begin{bmatrix} i^c_{td} \\ i^c_{tq} \end{bmatrix} + D \cdot \begin{bmatrix} v^c_{sd} \\ v^c_{sq} \end{bmatrix} \tag{C.13}$$

In equation C.13, the first term represents the PI controller action on the measured current, the second term includes the decoupling, and the last term denotes the voltage feed forward. Also note that, as the principle of superposition is used,

and the relation of interest is from system voltage to current output, the reference currents i_{td}^* and i_{tq}^* will be set equal to zero.

If delays or measurement filters are to be included in the model, they would be included as a multiplication of a scalar function in s. That is, the system voltage measurement vector v_s^c, would be multiplied with equations C.7 and C.9 as can be seen by inspection of figure C.1. Likewise, the current measurement vector i_t^c would be multiplied by equations C.7 and C.10. The control output voltage v_t^c would be multiplied by equation C.8 in the transition from control system reference frame to system reference frame. However, in the following deductions, this addition is suppressed as they are straightforward. This is done in order to limit the number of terms in the equations and retain clarity of the expressions. Therefore, any of the mentioned delays will simply be denoted D regardless of their origin.

In section 2.3.1, it was shown that the effect of the PLL could be included as an addition of a matrix in the transition from the actual system reference frame to the controller reference frame and vice versa. This is shown in equations C.14 to C.16.

$$\begin{bmatrix} i_{td}^c \\ i_{tq}^c \end{bmatrix} \approx \begin{bmatrix} 0 & I_q^s \cdot G_{PLL} \\ 0 & -I_d^s \cdot G_{PLL} \end{bmatrix} \cdot \begin{bmatrix} v_d^s \\ v_q^s \end{bmatrix} + \begin{bmatrix} i_{td}^s \\ i_{tq}^s \end{bmatrix} \tag{C.14}$$

$$\begin{bmatrix} v_d^c \\ v_q^c \end{bmatrix} \approx \begin{bmatrix} 0 & V_d^s \cdot G_{PLL} \\ 0 & -V_q^s \cdot G_{PLL} \end{bmatrix} \cdot \begin{bmatrix} v_d^s \\ v_q^s \end{bmatrix} + \begin{bmatrix} v_d^s \\ v_q^s \end{bmatrix} \tag{C.15}$$

$$\begin{bmatrix} m_d^c \\ m_q^c \end{bmatrix} \approx \frac{V_{DC}}{2} \begin{bmatrix} 0 & M_q^s \cdot G_{PLL} \\ 0 & -M_d^s \cdot G_{PLL} \end{bmatrix} \cdot \begin{bmatrix} v_d^s \\ v_q^s \end{bmatrix} + \begin{bmatrix} m_d^s \\ m_q^s \end{bmatrix} \tag{C.16}$$

Equation C.16 has been augmented to include the DC-voltage. This simplification can be seen by inspection of figure C.1 and remembering that the DC-voltage is assumed to be constant in this thesis.

Substituting equation C.16 into equation C.13 and rewriting, yields equation C.17.

$$\begin{bmatrix} v_{td}^s \\ v_{tq}^s \end{bmatrix} = D\frac{V_{DC}}{2} \begin{bmatrix} 0 & -M_q^s \cdot G_{PLL} \\ 0 & +M_d^s \cdot G_{PLL} \end{bmatrix} \cdot \begin{bmatrix} v_d^s \\ v_q^s \end{bmatrix} + D \cdot \begin{bmatrix} - \cdot H_{PI} & -L\omega_0 \\ L\omega_0 & - \cdot H_{PI} \end{bmatrix} \cdot \begin{bmatrix} i_{td}^c \\ i_{tq}^c \end{bmatrix} + D \begin{bmatrix} v_{sd}^c \\ v_{sq}^c \end{bmatrix} \tag{C.17}$$

From now on, let the matrices in equations C.14 to C.16 be denoted $\mathbf{G_{pll}^i}$, $\mathbf{G_{pll}^v}$, and $\mathbf{G_{pll}^m}$ as before. Also let the matrix in the second term of equation C.17 be denoted by $\mathbf{H}$ for compactness. Additionally, the vector variables will be given in bold type as before.

Equations C.14 and C.16 can also be substituted into equation C.17 to complete the transition from controller reference frame to system reference frame. This is shown in equation C.18.

$$\mathbf{v_t^s} = \frac{D \cdot V_{DC}}{2}\mathbf{G_{PLL}^m v_s^s} + \mathbf{H G_{PLL}^i v_s^s} + \mathbf{H} \cdot \mathbf{i_t^s} + D\mathbf{G_{PLL}^v v_s^s} + D\mathbf{v_s^s} \tag{C.18}$$

Substituting equation C.18 into equation C.12 and rearranging will finally yield equation C.19

$$\mathbf{i_t^s} = \alpha^{-1} \cdot (\beta + D \cdot (\frac{V_{DC}}{2}\mathbf{G_{PLL}^m} + \mathbf{G_{PLL}^v})) + (D-1) \cdot I) \cdot \mathbf{v_s^s} \tag{C.19}$$

where

$$\alpha = \left(\begin{bmatrix} sL+R & -L\omega_0 \\ L\omega_0 & sL+R \end{bmatrix} - D \cdot \begin{bmatrix} - \cdot H_{PI} & -L\omega_0 \\ L\omega_0 & - \cdot H_{PI} \end{bmatrix} \right) \tag{C.20}$$

and

$$\beta = \mathbf{H} \cdot \mathbf{G_{PLL}^i} \tag{C.21}$$

Thus, the equivalent output admittance of the converter model including delays and PLL effects are given in equation C.22.

$$\mathbf{Y_o} = -\alpha^{-1} \cdot (\beta + D \cdot (\frac{V_{DC}}{2}\mathbf{G_{PLL}^m} + \mathbf{G_{PLL}^v})) + (D-1) \cdot I) \tag{C.22}$$

Table C.1: *Variables used in analytical converter admittance calculations.*

Symbol	Variable
ω	Frequency variable
ω_0	Fundamental frequency of the grid
L	Filter inductior
V_{dc}	DC-side voltage
I_d	Steady state value of d-axis output current
I_q	Steady state value of q-axis output current
M_d	Steady state value of d-axis modulation signal
M_q	Steady state value of q-axis modulation signal
V_d	Steady state value of d-axis terminal voltage
V_q	Steady state value of q-axis terminal voltage
$K_{pll,i}$	Integral gain of the PLL controller
$K_{pll,p}$	Proportional gain of the PLL controller
$K_{c,i}$	Integral gain of the current controller
$K_{c,p}$	Proportional gain of the current controller
T_s	Switching period
ω_{vff}	Voltage feed-forward filter cutoff frequency
ω_{fbi}	Current feed-back filter cutoff frequency

Appendix D

MLBS Generation

The MLBS is a binary, deterministic, and periodic signal with period $T = P\Delta t$, where Δt is the time between each switching and P is an odd integer. The MLBS can be generated from a simple shift register with XOR feedback. Consider figure D.1 which depicts the first five blocks of a 15 bit shift register. The sequence is generated by collecting feedback from stage 1 and 4, and combining them through the exclusive-OR function (XOR). The XOR outputs 0 if the two inputs are equal and 1 otherwise, as shown in table D.1. Each stage, or box in the figure, is a memory unit that holds a value, passes it along, and stores the new inputted value at specified time steps.

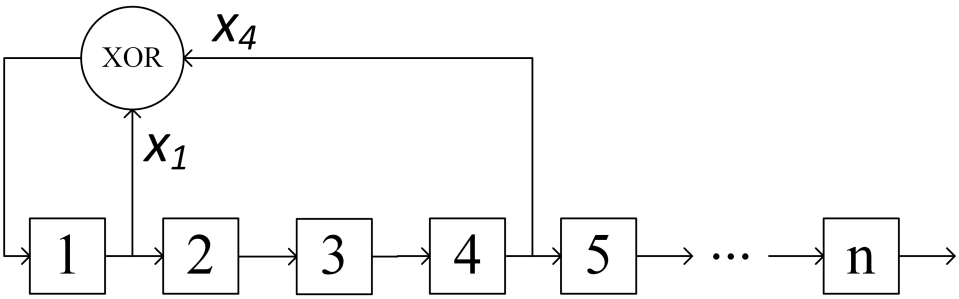

Figure D.1: 15-bit shift register with XOR feedback

As an example, the register is initialized from the number (0,0,0,1). The resulting sequence is shown in table D.2 below. From this, it can be seen that in time-step one, block 1 has passed through 0,0,0 and is storing the number 1. By moving through the time-steps the input of block 1 is generated from the previous output of blocks 1 and 4 and then passed through the shifts. It should be noted that every 4 digit binary number from (0,0,0,1) to (1,1,1,1) appears exactly once before

Table D.1: Evaluation of the XOR function

XOR	0	1
0	0	1
1	1	0

the sequence starts repeating itself after 15 steps. The number (0,0,0,0) may not appear as it would cause the shift register to only produce zeroes. Also note that the average of the output approaches zero as the sequence grows in length. If the inputs to the XOR were collected from, for example block 1 and 3, a 7 bit shift register would be created. This would output every binary number from (0,0,1) to (1,1,1) before starting to repeat itself after 7 shifts.

Table D.2: Example of a shift register output

$Time \setminus Block$	1	2	3	4
1	1	0	0	0
2	1	1	0	0
3	1	1	1	0
4	1	1	1	1
5	0	1	1	1
6	1	0	1	1
7	0	1	0	1
8	1	0	1	0
9	1	1	0	1
10	0	1	1	0
11	0	0	1	1
12	1	0	0	1
13	0	1	0	0
14	0	0	1	0
15	0	0	0	1
16	1	0	0	0
17	1	1	0	0

Bibliography

[1] United Nations. "Paris Agreement". In: (2015). URL: https://unfccc.int/sites/default/files/english_paris_agreement.pdf.

[2] European Commission. "Energy 2020: A strategy for competitive, sustainable and secure energy". In: (2010). URL: https://eur-lex.europa.eu/legal-content/EN/ALL/?uri=CELEX:52010DC0639.

[3] International Energy Agency. "World Energy Outlook 2016". In: ().

[4] P Brogan. "The stability of multiple, high power, active front end voltage sourced converters when connected to wind farm collector systems". In: (Jan. 2010).

[5] C. Buchhagen et al. "BorWin1 - First Experiences with harmonic interactions in converter dominated grids". In: *International ETG Congress 2015; Die Energiewende - Blueprints for the new energy age*. Nov. 2015, pp. 1–7.

[6] Garth D. Irwin, Amit K. Jindal, and Andrew L. Isaacs. "Sub-synchronous control interactions between type 3 wind turbines and series compensated AC transmission systems". In: *2013 4th IEEE International Symposium on Power Electronics for Distributed Generation Systems (PEDG)*. July 2011, pp. 1–6. ISBN: 978-1-4577-1000-1.

[7] C. Li. "Unstable Operation of Photovoltaic Inverter From Field Experiences". In: *IEEE Transactions on Power Delivery* 33.2 (Apr. 2018), pp. 1013–1015. ISSN: 0885-8977. DOI: 10.1109/TPWRD.2017.2656020.

[8] J. H. R. Enslin and P. J. M. Heskes. "Harmonic interaction between a large number of distributed power inverters and the distribution network". In: *IEEE Transactions on Power Electronics* 19.6 (Nov. 2004), pp. 1586–1593. ISSN: 0885-8993. DOI: 10.1109/TPEL.2004.836615.

[9] Tuomas Messo et al. "Real-Time impedance-based stability assessment of grid converter interactions". In: *2017 IEEE 18th Workshop on Control and Modeling for Power Electronics, COMPEL 2017* July (2017). DOI: 10.1109/COMPEL.2017.8013384.

[10] J. Machowski, J. Bialek, and J. Bumby. *Power System Dynamics: Stability and Control*. Wiley, 2011. ISBN: 9781119965053.

[11] A. Knop and F.W. W. Fuchs. "High frequency grid impedance analysis by current injection". In: *2009 35th Annual Conference of IEEE Industrial Electronics* (2009), pp. 536–541.

[12] J. Sun. "Impedance-Based Stability Criterion for Grid-Connected Inverters". In: *IEEE Transactions on Power Electronics* (2011).

[13] Xiongfei Wang, Frede Blaabjerg, and Weimin Wu. "Modeling and analysis of harmonic stability in an AC power-electronics-based power system". In: *IEEE Transactions on Power Electronics* 29.12 (2014), pp. 6421–6432.

[14] Wenchao Cao. "Impedance-Based Stability Analysis and Controller Design of Three-Phase Inverter-Based Ac Systems". PhD thesis. University of Tennessee, 2017.

[15] Jens G Balchen, Trond Andresen, and Bjarne A Foss. *Reguleringsteknikk*. 6. ed. Institutt for teknisk kybernetikk, NTNU, 2016.

[16] Amirnaser Yazdani and Reza Iravani. *Voltage-sourced converters in power systems : modeling, control, and applications*. IEEE Press/John Wiley, 2010.

[17] Ned Mohan and Tore M Undeland. *Power electronics: converters, applications, and design*. John wiley & sons, 2007.

[18] Bo Wen et al. "Influence of phase-locked loop on input admittance of three-phase voltage-source converters". In: *2013 Twenty-Eighth Annual IEEE Applied Power Electronics Conference and Exposition (APEC)*. IEEE. 2013, pp. 897–904.

[19] Antonino Riccobono, Markus Mirz, and Antonello Monti. "Noninvasive online parametric identification of three-phase AC power impedances to assess the stability of grid-tied power electronic inverters in LV networks". In: *IEEE Journal of Emerging and Selected Topics in Power Electronics* 6.2 (2017), pp. 629–647.

[20] Atle Rygg. "Impedance-based methods for small-signal analysis of power electronics dominated systems". PhD thesis. Norwegian University of Science and Technology, 2018.

[21] Mohamed Belkhayat. "Stability criteria for AC power systems with regulated loads". PhD thesis. Purdue University West Lafayette, NI, 1997.

[22] Mihai Ciobotaru, Vassilios Agelidis, and Remus Teodorescu. "Line impedance estimation using model based identification technique". In: *Power Electronics and Applications (EPE 2011), Proceedings of the 2011-14th European Conference on*. IEEE. 2011, pp. 1–9.

[23] Santiago Cobreces et al. "Grid impedance monitoring system for distributed power generation electronic interfaces". In: *IEEE Transactions on Instrumentation and Measurement* 58.9 (2009), pp. 3112–3121.

[24] Tomi Roinila, Matti Vilkko, and Jian Sun. "Broadband methods for online grid impedance measurement". In: *Energy Conversion Congress and Exposition (ECCE), 2013 IEEE*. IEEE. 2013, pp. 3003–3010.

[25] Mihai Ciobotaru et al. "Online grid impedance estimation for single-phase grid-connected systems using PQ variations". In: *Power Electronics Specialists Conference, 2007. PESC 2007. IEEE*. IEEE. 2007, pp. 2306–2312.

[26] Jason P Rhode, Arthur W Kelley, and Mesut E Baran. "Complete characterization of utilization-voltage power system impedance using wideband measurement". In: *IEEE Transactions on Industry Applications* 33.6 (1997), pp. 1472–1479.

[27] Tomi Roinila et al. “Designing MLBS excitation for the frequency-response measurement of AC-connected power electronics systems”. In: *IFAC Proceedings Volumes* 45.16 (2012), pp. 1329–1334.

[28] Mauricio Céspedes and Jian Sun. “Online grid impedance identification for adaptive control of grid-connected inverters”. In: *Energy Conversion Congress and Exposition (ECCE), 2012 IEEE*. IEEE. 2012, pp. 914–921.

[29] Daniel Martin, Enrico Santi, and Adam Barkley. “Wide bandwidth system identification of AC system impedances by applying pertubations to an existing converter”. In: *Energy Conversion Congress and Exposition (ECCE), 2011 IEEE*. IEEE. 2011, pp. 2549–2556.

[30] Keith Godfrey. *Perturbation signals for system identification*. Prentice Hall International (UK) Ltd., 1993.

[31] George C Verghese and VJ Thottuvelil. “Aliasing effects in PWM power converters”. In: *30th Annual IEEE Power Electronics Specialists Conference. Record.(Cat. No. 99CH36321)*. Vol. 2. IEEE. 1999, pp. 1043–1049.

[32] Douglas D Rife and John Vanderkooy. “Transfer-function measurement with maximum-length sequences”. In: *International Journal of Control* 37 (1989), pp. 419–444.

[33] Michael Jordan et al. “Frequency dependent grid-impedance determination with pulse-width-modulation-signals”. In: *Compatibility and Power Electronics (CPE), 2011 7th International Conference-Workshop*. IEEE. 2011, pp. 131–136.

[34] Peter Zörnig. *Nonlinear Programming: An Introduction*. Walter de Gruyter, 2014.

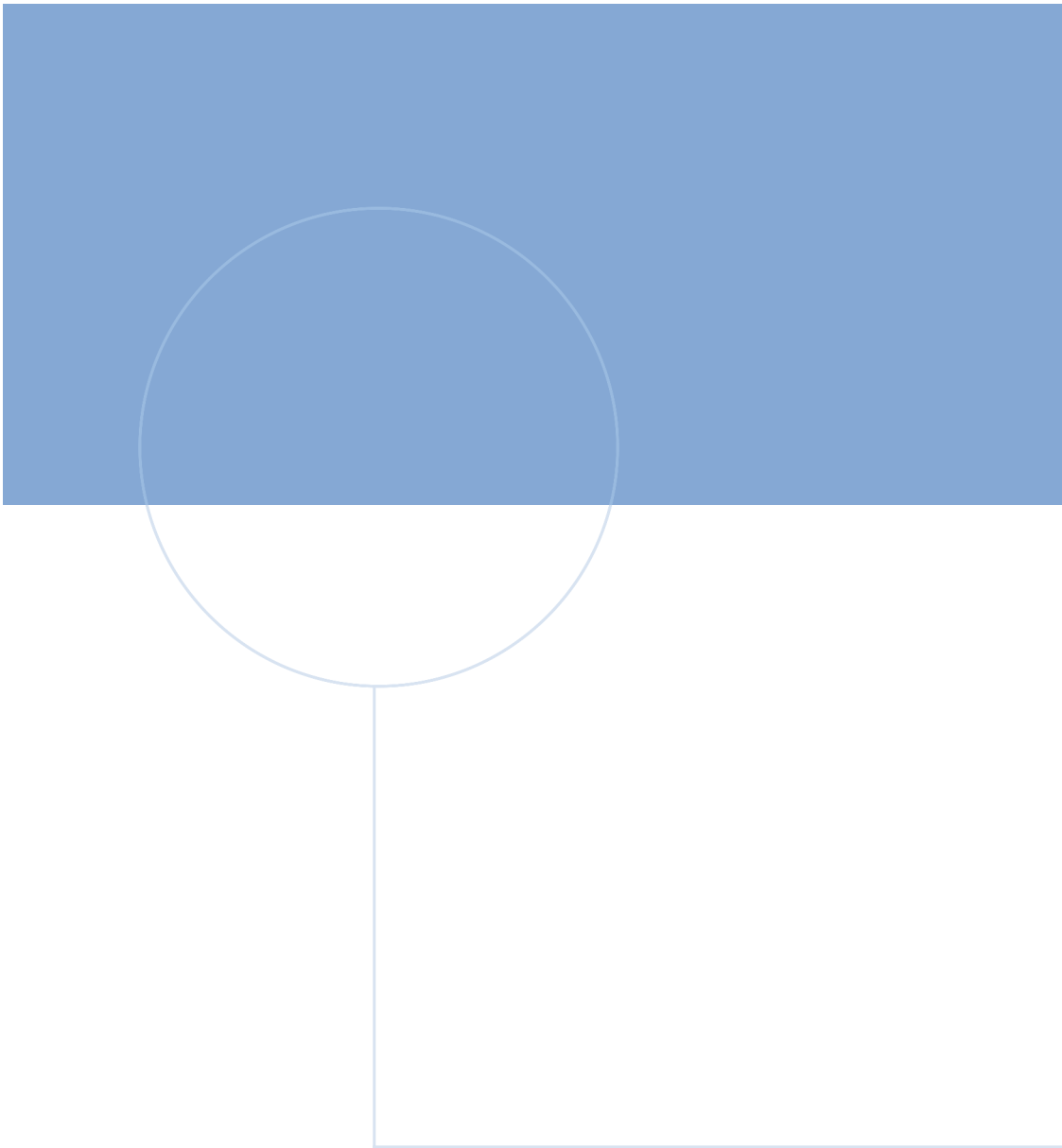

NTNU

Kunnskap for en bedre verden